

Detection of decametre-wavelength pulsed radio emission of 40 known pulsars

V. V. Zakharenko,¹★ I. Y. Vasylieva,¹ A. A. Konovalenko,¹ O. M. Ulyanov,¹
M. Serylak,^{2,3} P. Zarka,⁴ J.-M. Grießmeier,^{2,3} I. Cognard² and V. S. Nikolaenko¹

¹*Institute of Radio Astronomy of Nat. Acad. Sci. of Ukraine, Krasnoznamennaya 4, 61022 Kharkiv, Ukraine*

²*LPC2E, 3A, Avenue de la Recherche Scientifique, F-45071 Orléans cedex 2, France*

³*Station de radioastronomie de Nançay, Observatoire de Paris, CNRS/INSU, F-18330 Nançay, France*

⁴*LESIA, Observatoire de Paris, CNRS, UPMC, Université Paris Diderot, 5 Place Jules Janssen, F-92190 Meudon, France*

Accepted 2013 March 9. Received 2013 March 7; in original form 2012 August 20

ABSTRACT

The study of pulsars at the lowest radio frequencies observable from the ground (10–30 MHz) is complicated by strong interstellar (dispersion, scattering) and ionospheric (scintillation, refraction) propagation effects, as well as intense Galactic background noise and interference. However, it permits us to measure interstellar plasma parameters (the effects of which increase by a power of two to >4 times the wavelength), the spectrum and the pulse profile at low frequencies more accurately. Up to now, only ~10 pulsars have been successfully detected at these frequencies. The recent upgrade of the receivers at the Ukrainian T-shaped Radio telescope, second modification (UTR-2) has increased its sensitivity and motivated a new search for pulsed radio emissions. In this work we carried out a survey of known pulsars with declination above -10° , period >0.1 s and dispersion measure (DM) < 30 pc cm $^{-3}$, i.e. a sample of 74 sources. Our goal was either to detect pulsars not recorded before in the decametre range or to identify factors that prevent their detection. As a result, we have detected the radio emission of 40 pulsars, i.e. 55 per cent of the observed sample. For 30 of them, this was a first detection at these frequencies. Parameters of their average profiles have been calculated, including the intrinsic widening of the pulse (not due to interstellar scattering) with decreasing frequency. Furthermore, two pulsars beyond the selected DM (B0138+59 with DM ≈ 35 pc cm $^{-3}$ and B0525+21 with DM ≈ 51 pc cm $^{-3}$) were also detected. Our results indicate that there is still room to detect new transient and pulsed sources with low-frequency observations.

Key words: methods: data analysis – pulsars: general – pulsars: individual: PSR B0031–07.

1 INTRODUCTION

After the discovery of pulsars at 81.5 MHz (Hewish et al. 1968), the first pulsar detected at 40 MHz was PSR B1133+16 (Arecibo Observatory, 1968, unpublished). In 1969–1970 the pulsars PSR B1133+16 and B0809+74 were detected at 25 MHz (Bruck 1970). Systematic observations of pulsed radio emission in the decametre wavelength range started in 1972 after the commissioning of the Ukrainian T-shaped Radio telescope, second modification (UTR-2), near Kharkov, Ukraine, with an initial frequency range of 10–25 MHz (Braude, Megn & Sodin 1978). In 1973 the emission of three more pulsars was discovered (Bruck & Ustimenko 1973). Overall, only ~10 pulsars were detected at low frequencies until the late 1980s (Bruck & Ustimenko 1976; Bruck, Ulyanov &

Ustimenko 1986; Phillips & Wolszczan 1989). Large programmes and targeted studies were conducted between 25 and 40 MHz using radio telescopes such as the Arecibo dish (25 MHz, USA: Phillips & Wolszczan 1989), the Gauribidanur T-array (34.5 MHz, India: Deshpande & Radhakrishnan 1992, 1994), the DCR-1000 radio telescope (28–40 MHz, Pushchino, Russia: Izvekova et al. 1981) and Florida University’s 640-dipole array (26.3 MHz: Reyes et al. 1981).

Various characteristics of the low-frequency radio emission were investigated, including flux density, spectral index (with respect to higher frequency measurements), mean pulse profile and its variation with frequency (generally an increasing pulse width and sub-pulse separation with decreasing frequency; see e.g. Bruck 1987; Thorsett 1991). Also, the giant pulses of the Crab pulsar were detected in the decametre range (Popov et al. 2006), individual pulse characteristics and the subpulse structure of some pulsars were investigated (Ulyanov et al. 2007; Ulyanov, Zakharenko & Bruck

★ E-mail: zakhar@rian.kharkov.ua

2008; Ulyanov & Zakharenko 2012) and anomalous intensive pulses were discovered (Ulyanov et al. 2006).

Today, the largest metre-wave radio telescope, the Low-Frequency Array (LOFAR), is becoming operational (van Haarlem et al., in preparation) and one of its key science cases is the study of pulsars and transient radio sources (Stappers et al. 2011). The frequency range of the telescope is divided into two bands. The low-band antennae cover the range 10–90 MHz, although they are optimized for frequencies above 30 MHz (Stappers et al. 2011; van Haarlem et al., in preparation). In contrast, UTR-2 can operate in the band 8–40 MHz (it is now the world’s largest radio telescope in this range) but it is most sensitive at frequencies below 25 MHz. Therefore joint observations (simultaneous or not) will be highly beneficial, providing a continuous frequency coverage from 8–240 MHz.

At present, only a small number of pulsars have been detected in the decametre wavelength range, which can lead to erroneous conclusions about pulsar properties at low frequencies. In order to improve this situation, we took advantage of the substantial improvement in sensitivity provided by the modernized receiver system at UTR-2 (Ryabov et al. 2010; Konovalenko et al. 2011) in order to increase the sample of low-frequency pulsars. We start with a survey of all known pulsars that are visible from this telescope (located at longitude = 36°56′29″E, latitude = +49°38′10″). Where detection fails, we try to identify the factors that prevented detection.

1.1 Challenges and advantages of observing pulsed signals at low frequencies

The lower bound of the radio transparency window of Earth’s ionosphere is determined by a critical frequency of about 10 MHz. In the lowest two octaves above this frequency, research into pulsed and transient radio emission is complicated by a number of hindering factors. The most serious obstacle is the growth of the scattering time due to propagation through the interstellar medium (ISM) towards lower frequencies $\propto \nu^{\alpha_{\text{sc}}}$, with $\alpha_{\text{sc}} = -4.4$ for a Kolmogorov distribution of inhomogeneities and ν the frequency of observation. This leads to an increase of the scattering time between the decametre range ($\nu = 25$ MHz) and the decimetre range ($\nu = 1$ GHz) by a factor $(25/1000)^{-4.4} \approx 10^7$. At low frequencies, the pulses are broadened so much that they start to overlap, washing out the contrast between intensity maxima and minima. This is most striking when the pulse period is short with respect to the scattering time. For example, for the Crab pulsar ($P \approx 0.033$ s) at 25 MHz the scattering time is expected to be about 30 s. Actual measurements of the scattering time of giant pulses (Popov et al. 2006) gave values of about 3 s, still 100 times larger than the pulsar period. Regular pulses of the pulsar were thus not detected. Even the detection of long-period pulsars becomes extremely difficult when they are distant and strongly scattered.

The next serious hindering factor is the growth of Galactic background noise towards lower frequencies $\propto \nu^{-2.5}$ down to ≈ 5 MHz (Ellis 1982), with a brightness temperature reaching 550 000 K at 8 MHz outside the Galactic disc and values several times higher in the Galactic plane (Milogradov-Turin & Smith 1973; Caswell 1976; Roger et al. 1999).

Another difficulty is the scintillation in the ionosphere, quite strong at low frequencies and resulting in undesirable intensity modulations of received radio emission. The combined influence of scintillation and refraction leads to fluctuations of the apparent position of a source even when it is situated near the zenith. For

UTR-2, the mean position error is 0.1 and the maximum error is ≥ 0.7 (Braude et al. 2002), larger than the beam width of UTR-2 at 25 MHz (0.5). In addition, the intrinsic sporadicity of pulsar radiation appears to increase towards lower frequencies (Ulyanov et al. 2006). Therefore, obtaining a stable shape of the average pulse profile requires observations of longer duration.

An instrumental factor that limits the sensitivity reachable in the range 10–30 MHz is the small absolute observation bandwidth. The sensitivity is proportional to the square root of the frequency bandwidth but, due to the frequency dependence of the pulsar emission and of the noise parameters, integration over a broad frequency band should be avoided in this range.

Let us estimate the signal-to-noise ratio (S/N) deterioration for two frequencies 25 and 100 MHz, separated only by two octaves. It is well known that the majority of pulsars have a turnover in their spectrum at metre wavelengths. At lower frequencies, the flux density falls off with spectral index α varying within wide limits 0–4; see e.g. Malofeev, Malov & Shchegoleva (2000) and Maron et al. (2000). Thus, pulsar fluxes for the aforementioned frequencies and a moderate value of $\alpha = 1$ will differ by a factor of 4. Moreover, due to the increase of Galactic background noise by a factor $(25/100)^{-2.5} = 32$, the resulting S/N is reduced by more than two orders of magnitude.

Finally, interference from broadcast radio stations may exceed astronomical signals by up to 70–80 dB (especially during the daytime) and propagation through the ionosphere can further reduce the S/N by a small factor. Taken together, these reasons explain why only a relatively small number of pulsars has been detected at the lowest frequencies so far.

Despite all these difficulties, the decametre range remains quite attractive, especially due to the above pulse profile broadening, which leads to a significant increase of the beaming fraction in the 10–30 MHz range in comparison with 1.4-GHz surveys. There are also indications for some pulsars of the presence in the decametre wavelength range of a wide, low-intensity ‘plateau’ in addition to the pulse (see e.g. Phillips & Wolszczan 1989).

Another factor is that some pulsars such as PSR B0943+10 are characterized by a steep spectral index, i.e. a flux density strongly increasing at low frequencies. This increases the probability of discovering new sources at very low frequencies.

The aforementioned strong frequency dependence of parameters such as the dispersion and the rotation measure allows us to determine them very accurately in the decametre range. The dispersion delay is given by (Backer et al. 1993)

$$\Delta t = 10^{16} \text{DM} / 2.410331 (\nu_{\text{min}}^{-2} - \nu_{\text{max}}^{-2}). \quad (1)$$

This quadratic dependence on wavelength permits us to measure the dispersion measure (DM) very accurately. It also allows us to distinguish clearly between single pulses, even from the closest sources, and broad-band terrestrial interference. Indeed, a very small DM of 0.1 pc cm^{−3} gives a signal propagation delay of about 1.14 s between frequencies of 16.5 and 33.0 MHz. This exceeds the pulse width of all known pulsars. For high-frequency observations, the distinction between a truly zero DM and a DM of a few pc cm^{−3} is a significant problem (see e.g. Kondratiev et al. 2009). The presence of dispersion in the signal can be especially valuable for the detection of signals from nearby transient radio sources, because frequency-dependent dispersion is one of the main characteristics allowing us to distinguish them from broad-band interference of terrestrial origin.

Similarly, magnetic field variations along the line of sight will be easier to detect at low frequencies because of the quadratic dependence of Faraday rotation on wavelength.

Irregular low scattering with an exponent $\alpha_{\text{SC}} < 4$, observed for giant pulses of the Crab pulsar, was confirmed in Bhat et al. (2007) as an exceptional event. The results of Popov et al. (2006) show that at very low frequencies, thanks to this irregular low scattering, not only close transient signals but also sources with DM up to 60 pc cm^{-3} can be detected.

Using the model of galactic electron concentration by Cordes & Lazio (2002), this maximum DM translates into a maximum distance $\geq 2 \text{ kpc}$ in the Galactic plane and up to the borders of the Galactic disc in the direction of the poles. This restriction to relatively close sources makes the limitation in S/N imposed by intense low-frequency Galactic background noise less constraining.

This is why the decametre range can be very favourable for the study of transient phenomena and can help to provide answers to important open questions, for example

(i) an explanation of the discrepancy between supernova explosion rates measured by gamma-ray emission of radioactive aluminium (^{26}Al) of the Galaxy (Diehl et al. 2006) and the number of various remnants of these explosions (Keane & Kramer 2008); the latter can be significantly increased by the recently discovered Rotating Radio Transients (RRATs) (McLaughlin et al. 2006);

(ii) verification of contradictory data regarding the existence of radio emission from X-ray Dim Isolated Neutron Stars (XDINS) (Malofeev, Malov & Teplykh 2005; Kondratiev et al. 2009; Zakharenko, Markova & Vasylieva 2011);

(iii) better constraints for the neutron-star radio-emission mechanism.

1.2 Maximizing the sensitivity of the pulsar search at the radio telescope UTR-2

Since the upgrade of the preamplification system (Abranin et al. 2001), receiver noise is negligible in comparison with the above values of the sky temperatures. Evolution of backends towards digital receivers (Lecacheux et al. 1998; Zakharenko et al. 2007) led after 2006 to a new generation of digital receivers (hereafter DSPZ), the characteristics of which are described in (Kozhin, Vynogradov & Vavriv 2007; Ryabov et al. 2010; Konovalenko et al. 2011). DSPZ receivers can record the entire band of the radio telescope at once. Thus, we can compute the maximum sensitivity S achieved for a given collecting area. We have chosen the 4σ level (here, σ is standard deviation) as the maximum intensity radiated by non-detected sources (as in Kondratiev et al. 2009; Zakharenko et al. 2011). This level is given by the formula

$$S = \frac{4 \times (2kT)}{A_e(z) \sqrt{\Delta\nu \Delta t (t_i/P)}}, \quad (2)$$

with k the Boltzmann constant, T the galactic background temperature, $A_e(z)$ the collecting area of the telescope ($150\,000 \text{ m}^2$ in the zenith direction), $\Delta\nu$ the frequency band of observations, Δt the integration time and (t_i/P) the fraction of time occupied by the pulse itself, which is of duration t_i , relative to the pulsar period P . Assuming $T \approx 20\,000 \text{ K}$, $A_e \approx 100\,000 \text{ m}^2$ (taking into account the geometrical factor for off-zenith sources), $\Delta\nu = 16.5 \text{ MHz}$, $\Delta t = 5400 \text{ s}$ and $(t_i/P) = 0.05$, the resulting sensitivity is about 33 mJy . Actually, due to scintillations in the ionosphere, the effect of nulling and the more sporadic nature of pulsar emission at low frequencies compared with higher ones, this estimate of the sensitivity should

be considered as an optimistic one. If we consider the possibility of individual pulse detection, the product $\Delta t (t_i/P)$ in expression (2) must be replaced by $\Delta t = 0.1 \text{ s}$, the pulse width expected for RRATs or giant pulses of pulsars. Then the detection limit is approximately 1.6 Jy . This can be regarded conversely as a pessimistic estimate, since for a large fraction of RRATs or giant pulses we can expect a few pulses per observational period.

In searches for decametre radio emission from XDINSs (Zakharenko et al. 2011), sensitivities of a few mJy were achieved. This makes us hope that the improved instrumentation capabilities will give us a better chance of detecting pulse radiation from objects that have not been detected previously. However, the total number of detected pulsars in the decametre range will depend on the extent to which they are affected by the limiting factors discussed in Section 1.1.

Therefore, the motivation for the observations presented here is to answer the question: how many known pulsars can be detected in the decametre range in comparison with higher frequency observations? In addition, we tried to identify factors that prevent us from detecting a pulsar and find ways to reduce their impact.

The structure of this article is as follows. Section 2 describes the instrumentation and method of observation. Section 3 presents the results of the observations, which are discussed in Section 4. Section 5 presents our conclusions.

2 INSTRUMENTATION AND OBSERVATIONS

The good interference immunity of UTR-2 enables round-the-clock observations even in a polluted situation. To have good sensitivity, the effective area of the telescope must be sufficiently high, so we chose sources with declination $\delta > -10^\circ$, such that the decrease of A_e due to geometrical projection is less than a factor of two (the latitude of UTR-2; see Section 1). In the numerical application of equation (2) above, we used the average $A_e(z)$ for the current survey. Another important parameter is the time resolution. Its selection (8 ms) supposes that only a few of the known nearby pulsars (B0950+08, B0809+74) have a lower scattering time at decametre wavelengths. Taking into account this fact and the known scattering time constants for other pulsars, we fixed a minimum period of 100 ms for the observed pulsars. For the survey we chose bounds of $\text{DM} = 0\text{--}30 \text{ pc cm}^{-3}$.

In 2010 October, the Australia Telescope National Facility (ATNF) pulsar data base (Manchester et al. 2005) contained 74 pulsars satisfying these criteria.

It is well known that high DM accuracy is a crucial factor to determine the shape of the average profile and to calculate several physical parameters of the pulsar's radio emission. The trial DM step has to be chosen such that the intensity decrease between an analysis with the best trial DM and with the precise value of the DM remains low. According to expression (12) of Cordes & McLaughlin (2003), the ratio of fluxes at inexact DM ($F_{\delta\text{DM}}$) and at the true DM (F) can be written as

$$\frac{F_{\delta\text{DM}}}{F} = \frac{\sqrt{\pi}}{2} \zeta^{-1} \text{erf } \zeta, \quad (3)$$

where $\zeta = 6.91 \times 10^{-3} \delta\text{DM} (\Delta\nu_{\text{MHz}})/(W_{\text{ms}} \nu_{\text{GHz}}^3)$, with ν the central frequency of observation, $\Delta\nu$ the bandwidth and W_{ms} the pulse width. In order to keep this ratio below 5 per cent for $\Delta\nu = 16.5 \text{ MHz}$, $\nu = 0.024 \text{ GHz}$ and $W = 100 \text{ ms}$, a maximum error $\delta\text{DM} = 0.005 \text{ pc cm}^{-3}$ can be tolerated.

To determine the DM with the highest possible accuracy, the trial DM step should be chosen to be as small as possible. For our data, its

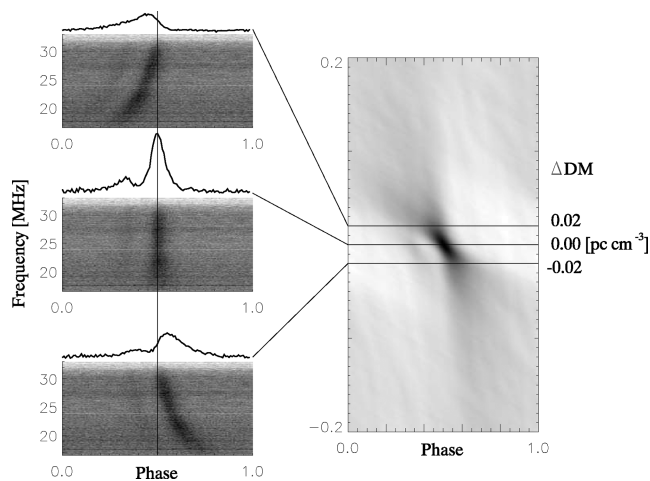


Figure 1. An example of determination of the DM in the band 16.5–33.0 MHz for the pulsar PSR B0031–07. The grey-scale image to the right represents the average pulse profile versus rotational phase and dispersion measure. The slope of the region of maximum intensity is induced by the fact that the compensation of dispersion delay is related to the upper frequency of the range. ‘Undercompensation’ ($\Delta\text{DM} < 0$) shifts the average profile to a later phase of the pulsar rotation period, while ‘overcompensation’ ($\Delta\text{DM} > 0$) shifts it to an earlier phase (left panels).

value has a lower threshold related to the available time resolution: adjacent trial DMs should correspond to a relative time delay at the lowest frequencies of at least one time bin (8 ms). We used a step width of $\Delta\text{DM} = 0.002 \text{ pc cm}^{-3}$ (corresponding to a shift of 2.5 time bins at the lowest frequencies).

To illustrate the search for a refined DM, we show intermediate and final data for PSR B0031–07. Fig. 1 shows the results of compensation of dispersive propagation delay with different values of the trial DM. The left panel shows interference-free and accumulated dynamic spectra over 5700 periods of the pulsar, in the frequency range 16.5–33.0 MHz. On the top of each of the three panels the averaged and frequency-integrated pulse profile of the pulsar is shown. Each profile corresponds to a horizontal cut of the grey-scale image in the right panel (at a specific value of the trial DM). Profiles are shown with a pitch of 0.02 pc cm^{-3} . The pulse profile with the maximum S/N, which occurs for a good vertical alignment of pulse components at all frequencies of the dynamic spectrum, corresponds to the best compensation of the dispersion delay.

In our algorithm, the compensation of the dispersion delay is calculated with respect to the highest frequency channel. This defines the slope of the region of maximum intensity in the ‘rotational phase–dispersion measure’ plane (right side panel of Fig. 1). When deviating from the optimal DM towards negative ΔDM (‘undercompensation’), the maximum of the average profile decreases and shifts to a later phase of the period (Fig. 1, left lower panel), while an ‘overcompensation’ ($\Delta\text{DM} > 0$) causes a shift to an earlier phase (Fig. 1, left upper panel).

The lower the frequency and the broader the measurement bandwidth, the more accurate is the determination of the DM, as follows from equation (3). Fig. 2 shows three images of the ‘rotational phase–dispersion measure’ plane for PSR B0031–07, with integration over different frequency ranges (from left to right: $\Delta\nu = 1, 4$ and 16 MHz) around the same centre frequency of 25 MHz. One can see that the size of the high-intensity region increases for a narrower bandwidth of observations. At the same time, the maximum deviation from the optimal DM that allows us to detect a pulsar

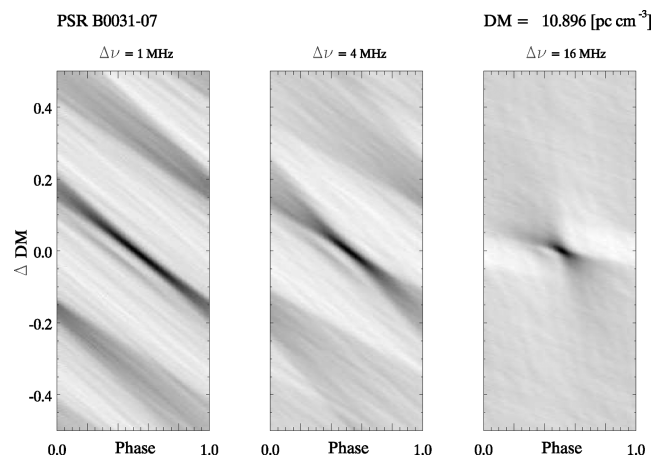


Figure 2. ‘Rotational phase–dispersion measure’ plane with integration over frequency ranges $\Delta\nu$ of 1 MHz (left panel), 4 MHz (middle panel) and 16 MHz (right panel). The size of the maximum intensity region increases when the bandwidth decreases, allowing us to detect a pulsar with larger deviations of DM from the optimum value but leading to a DM measurement with less accuracy.

also increases. Maximizing the observational bandwidth thus leads to better accuracy in determining the DM, but its inaccurate choice will not allow us to detect a pulsar (if the high-intensity region falls outside the explored DM range). However, if too wide a bandwidth is taken then the frequency evolution of the pulse profile can affect the DM value (Hassall et al. 2012).

The choice of frequency band is related to the transparency of the ionosphere and to the interference situation. In the morning, afternoon and evening, the conditions are acceptable only for observations at frequencies above 14–16 MHz. At night, observations down to 8 MHz can be conducted, because the interference level is low. Due to round-the-clock observations, the frequency range for our survey was chosen between 16.5 and 33.0 MHz. In spectral mode, the DSPZ receiver has 4096 frequency channels in this range, each of approximately 4 kHz width. Each pulsar was observed for 90 min. During this interval, 1800–25 000 periods have been accumulated, depending on the pulsar period (see Table 1). We used incoherent dedispersion, i.e. in the time–frequency plane after detection, which broadens the signal by no more than 100 ms for $\text{DM} = 30 \text{ pc cm}^{-3}$ even in the lowest frequency channel, where the majority of pulsars have negligibly low radiation.

The depth of radio frequency interference (RFI) cleaning can be varied in our interference-removal algorithm, depending on interference conditions. Masking affected frequency channels and/or time intervals leads to an unavoidable loss of samples where pulsar radiation is present. Therefore, we applied less deep cleaning for night-time observations. For the data obtained during the day-time (Fig. 3), when the interference levels exceeded the levels of unaffected channels by tens of dB a deeper cleaning was applied.

The cleaning procedure consists of several stages. First, in the narrow-band (4 kHz) spectral channels the standard deviation (σ_{ch}) is calculated iteratively by discarding the values exceeding $3\sigma_{\text{ch}}$ at each step (with a stop criterion corresponding to consecutive values of σ_{ch} differing by no more than 10^{-5}). The resulting value is used to determine two thresholds of cleaning. The first one (usually between $4\text{--}6\sigma_{\text{ch}}$) is the clipping level. This mode is useful when a relatively strong pulsar signal overlaps with low-intensity interference or a background-noise peak due to the scintillations of a nearby point source (this situation occurs quite often because of the relatively

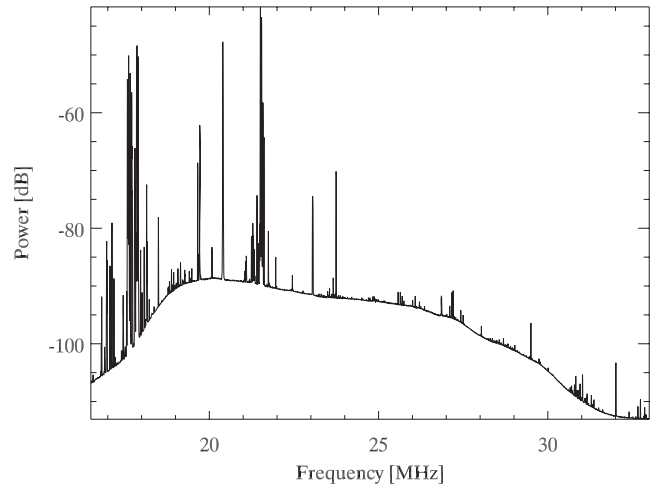
Table 1. DM values given in the catalogue of Manchester et al. (2005) and obtained during the present work at UTR-2 for the 40 detected pulsars.

No	Name	DM* (pc cm ⁻³)	DM (UTR-2) (pc cm ⁻³)	<i>P</i> (s)	Number of <i>P</i>
1	B0031–07	11.38(8)	10.896(4)	0.943	5726
2	J0051+0423	13.9(1)	13.936(3)	0.355	15 211
3	B0053+47	18.09(4)	18.144(8)	0.472	11 440
4	B0148–06	25.66(3)	25.661(12)	1.465	3686
5	B0320+39	26.01(3)	26.162(11)	3.032	1781
6	B0329+54	25.66(3)	25.661(11)	0.714	7563
7	B0450+55	14.495(7)	14.602(5)	0.341	15 835
8	B0809+74	6.116(18)	5.755(3)	1.292	4179
9	B0823+26	19.454(4)	19.484(6)	0.531	10 169
10	B0834+06	12.889(6)	12.872(4)	1.274	4238
11	B0919+06	27.271(6)	27.316(6)	0.431	12 529
12	J0927+23	23(2)	24.032(10)	0.762	7086
13	B0940+16	20.32(5)	20.354(8)	1.087	4967
14	B0943+10	15.4(5)	15.339(4)	1.098	4918
15	B0950+08	2.958(3)	2.972(2)	0.253	21 343
16	B1112+50	9.195(8)	9.185(4)	1.656	3260
17	B1133+16	4.864(5)	4.846(2)	1.188	4545
18	J1238+21	17.5(1.2)	17.968(5)	1.119	4825
19	B1237+25	9.242(6)	9.268(2)	1.382	3907
20	B1322+83	13.312(18)	13.312(4)	0.670	8059
21	B1508+55	19.613(20)	19.622(9)	0.740	7297
22	B1530+27	14.698(18)	14.706(3)	1.125	4800
23	B1540–06	18.403(4)	18.334(100)	0.709	7616
24	B1604–00	10.682(5)	10.688(2)	0.422	12 796
25	B1612+07	21.39(3)	21.402(14)	1.207	4473
26	B1633+24	24.32(4)	24.540(8)	0.491	10 997
27	J1741+2758	29.3(6)	29.146(18)	1.361	3967
28	B1822–09	19.38(4)	19.408(21)	0.769	7022
29	B1839+56	26.698(11)	26.804(6)	1.653	3266
30	J1851–0053	24(4)	24.556(37)	1.409	3832
31	J1908+0734	11.104(11)	11.234(50)	0.212	25 471
32	B1919+21	12.455(6)	12.435(4)	1.337	4038
33	B1929+10	3.180(4)	3.180(2)	0.227	23 788
34	B1944+17	16.220(16)	15.720(4)	0.441	12 244
35	B1952+29	7.932(7)	7.870(5)	0.427	12 646
36	B2016+28	14.172(4)	14.200(7)	0.558	9677
37	B2110+27	25.113(4)	25.114(18)	1.203	4488
38	J2307+2225	7.08(3)	6.842(12)	0.536	10 074
39	B2310+42	17.2758(13)	17.256(15)	0.349	15 472
40	B2315+21	20.906(7)	20.904(13)	1.445	3737

*Manchester et al. (2005).

wide antenna pattern). Moreover, such scintillations usually amplify not only the signal of the point source but also the pulsar signal. In order not to discard the corresponding measurements, we clip the signal level but retain it in subsequent analysis). However, if a signal is extremely strong in a single DSPZ channel, it is almost certainly interference. Therefore, the second threshold (usually at $6\text{--}10\sigma_{\text{ch}}$) corresponds to the elimination of high-intensity signals. This step actually removes efficiently intense broad-band interference. In summary, values below the first threshold are left unaltered, values between the first and the second threshold are clipped and values above the second threshold are removed (blanked).

During the daytime we need to eliminate more frequency channels affected by interference from broadcast and specialized radio stations. For that purpose, we compare the average power in each channel with that in adjacent channels. Using the same iterative algorithm as above, the standard deviation σ_{sp} of unpolluted frequency channels (averaged during ≈ 10 s) is calculated. Then, all

**Figure 3.** Example of spectrum received by UTR-2 during the daytime, affected by strong interference.

channels with average level exceeding a given threshold (usually $4\sigma_{\text{sp}}$) are excluded from the analysis.

Furthermore, low-intensity broad-band interference often occurs in the range 27–33 MHz during the daytime. To eliminate this, another specific cleaning stage is applied. The previously cleaned dynamic spectra are integrated versus frequency and the σ_{sum} of the resulting time series is calculated. Time intervals with intensity exceeding $4\sigma_{\text{sum}}$ are also excluded. When calculating pulsar fluxes, the information on the number of retained frequency channels and time intervals is taken into account.

We conducted three sessions of observations (2010 October 11–18, 2011 January 17–24 and 2011 March 21–28). During the first session, all 74 pulsars were observed. During the second and the third sessions, those sources that were not detected in the previous session were reobserved. The third session was also used to observe some pulsars with $\text{DM} \geq 30 \text{ pc cm}^{-3}$.

3 RESULTS

For the first time, 40 pulsars known from higher frequency observations have been detected in the decametre wavelength range. For only 10 of these have decametre data previously been published. After determining accurately each pulsar's DM and average flux density, its spectral index was computed from the pulsar's known spectral maximum in flux density and our decametre-wavelength measurements. Also, the widths of the average pulse profiles at 50 per cent and 10 per cent levels relative to its maximum intensity and the scattering time constant at 25 MHz have been determined. Power-law indices for the scattering time constant have been calculated with respect to the catalogue data at 1 GHz. For the 34 non-detected pulsars (out of our sample of 74), upper limits on the flux density corresponding to the 4σ level have been obtained.

3.1 Refining the dispersion measure

Figs A1 and A2 in the Appendix show average profiles and grey-scale images of the 'rotational phase–dispersion measure' plane for all detected pulsars. Fig. A1 shows the average profiles of 15 pulsars with high S/N at 25 MHz (over the band 23–27 MHz, bold curve) and at 20 MHz (over the band 18–22 MHz, thin curve). We chose to restrict our focus to 4-MHz bandwidths whenever permitted by the S/N in order to avoid smearing due to the intrinsic variation

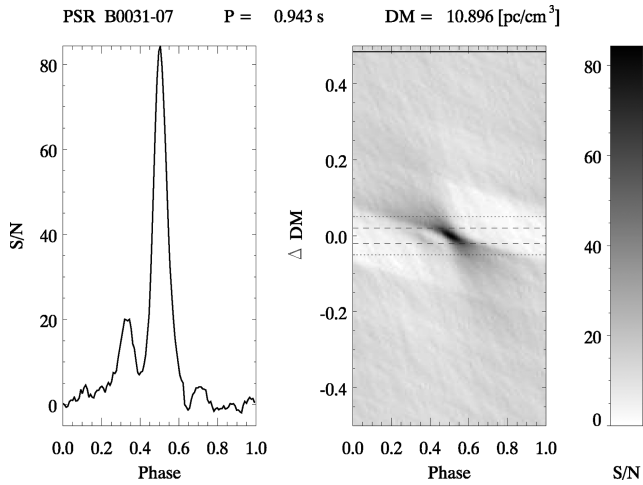


Figure 4. Average profile corresponding to the optimal DM for PSR B0031–07, after integration over the frequency range 23–27 MHz (left panel). The grey-scale image displays the profiles obtained for different DMs, over the band 16.5–33 MHz (right panel). The S/N decreases by a factor of 2 and by a factor of 10 within ± 0.02 (dashed line) and ± 0.05 (dotted line) pc cm^{-3} of the optimal DM, respectively. The bold line indicates the DM value from the catalogue of Manchester et al. (2005). It is impossible to detect a pulsar with such a DM value in broad-band low-frequency observations.

of the average pulse profile with frequency. For the 25 pulsars depicted in Fig. A2, the S/N in a band of 4 MHz was too low and therefore the average profile is obtained over the band 20–32 MHz (or 16.5–33.0 MHz for PSRs B0148–06, J1238+21, B0940+16 and B1822–09).

Let us consider the case of PSR B0031–07 shown in Fig. 4 as an example. The left panel shows the average pulse profile, obtained by stacking of all pulses during 90 min of observation integrated over the band 25 ± 2 MHz. The right panel shows the grey-scale intensity image of the accumulated signal of the pulsar as a function of the DM. To improve the accuracy of the DM determination for all pulsars, the full observational band (16.5–33 MHz) has been used. We evaluated error bars for DM as the intervals in which the S/N decreases by 5 per cent, by a factor of 2 and by a factor of 10, respectively. The size of these intervals for each pulsar depends on several factors, including the average profile shape, the pulse width, the noise level in the off-pulse area, etc. For the case of PSR B0031–07, the latter two intervals are about ± 0.02 and $\pm 0.05 \text{ pc cm}^{-3}$. In Fig. 4 they are marked by dashed and dotted lines respectively. The DM value for this pulsar (11.38 pc cm^{-3}) specified in the catalogue (Manchester et al. 2005) is marked in Fig. 4 with a bold line. It is obviously not appropriate for our low-frequency broad-band measurements. At this DM value, the decametre pulsar signal is smeared and weakened to such an extent that it becomes impossible to distinguish the pulse component from the off-pulse area. Our measurements ($10.896 \pm 0.004 \text{ pc cm}^{-3}$) confirm the conclusion of Karuppusamy, Stappers & Serylak (2011) that for PSR B0031–07 the DM value and the rate of DM change given by Hobbs et al. (2004) and Manchester et al. (2005) are likely to be incorrect. Also, for PSR B0809+74, regularly observed at UTR-2, $\text{DM} = 6.116 \pm 0.018 \text{ pc cm}^{-3}$ in (Hobbs et al. 2004) is not consistent with our measurements. For some of the pulsars the error bars given in the catalogue are quite large (for example, for PSR J0927+23). Therefore, we used the data from Manchester et al. (2005) as a starting value and searched in a DM

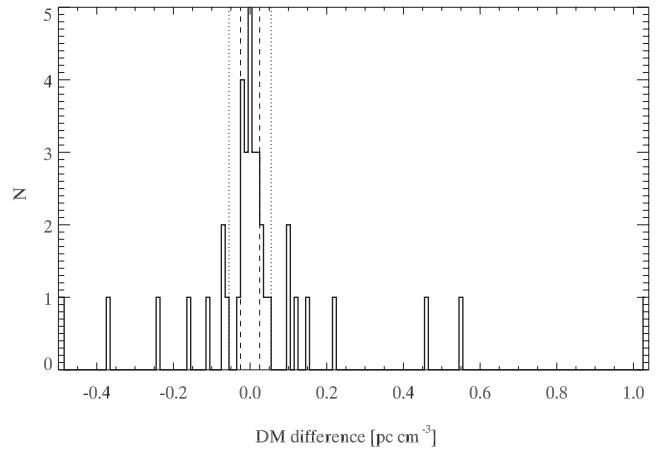


Figure 5. Histogram of DM differences between UTR-2 measurements and those of Manchester et al. (2005), along with the limits at ± 0.02 and $\pm 0.05 \text{ pc cm}^{-3}$.

interval of ± 10 per cent around the specified value. This range is wide enough and may include even the largest time variations of the DM (Phillips & Wolszczan 1992; Hobbs et al. 2004; Karuppusamy et al. 2011).

The DMs that we have determined at UTR-2 are listed in Table 1 and compared with the values from the catalogue of Manchester et al. (2005). The errors in our DM values were estimated as the interval over which the S/N ratio drops by 5 per cent.

We have analysed the differences in DMs between our results and catalogue values. The results are shown in Fig. 5, as a histogram of the number of pulsars versus the DM differences. ΔDM lies within $\pm 0.02 \text{ pc cm}^{-3}$ for 14 pulsars, within $\pm 0.05 \text{ pc cm}^{-3}$ for 24 pulsars and above $\pm 0.05 \text{ pc cm}^{-3}$ for 16 pulsars.

While our average DM values agree well with those listed in the catalogue Manchester et al. (2005), the standard deviations of the DM differences of Fig. 5 notably exceed our error bars for DM determination from decametre measurements. For example, the average value of the DM differences in Fig. 5 is 0.025, whereas the standard deviation is 0.248 pc cm^{-3} . If we exclude the pulsars with the largest errors in Manchester et al. (2005) (PSR J0927+23 and PSR J1851–0053; see Table 1), as well as PSR B0809+74, for which the DM in other catalogues (Taylor, Manchester & Lyne 1993) is closer to our value than that of Manchester et al. (2005), the average value is -0.006 and the standard deviation is 0.154 pc cm^{-3} . In both cases, the standard deviation of ΔDM is several times larger than the error in our measurements.

This illustrates the importance of low-frequency measurements for future redetection or new searches of pulsars, to determine accurately DMs as well as rotation measures, average pulse width and other related characteristics (DM change rate, etc.). Based on the above refined DMs, we can now estimate the S/N, flux densities and spectral indices of the 40 detected pulsars.

3.2 Flux densities and spectral indices

Flux densities of detected pulsars and upper detection limits for non-detected ones have been determined on the basis of equation (2), taking into account the following considerations: in a band of one octave, the values of the background temperature, telescope effective area or pulsar flux density cannot be regarded as constants. However, without integration in frequency it is impossible to achieve the required sensitivity. We have therefore chosen a compromise:

Table 2. Flux density of strong pulsars detected at two frequencies and spectral indices α_{20-25} and $\alpha_{25-\nu_{\max}}$. The maximum error in spectral indices is $\sim \pm 1.8$.

N	Pulsar	Flux (mJy) (20 MHz)	Flux (mJy) (25 MHz)	α_{20-25}	Flux (mJy) (ν_{\max})	$\alpha_{25-\nu_{\max}}$
1	B0031-07	353 ± 106	345 ± 104	-0.1	$560 \pm 310^*$ (102.5 MHz)	0.34
2	B0053+47	34 ± 11	100 ± 30	4.83	$80 \pm 26^*$ (102.5 MHz)	-0.16
3	B0809+74	1300 ± 390	1190 ± 360	-0.4	$1870 \pm 350^{**}$ (61 MHz)	0.51
4	B0823+26	186 ± 56	203 ± 61	0.39	$1070 \pm 560^{**}$ (85 MHz)	1.36
5	B0834+06	291 ± 88	329 ± 99	0.55	$2090 \pm 420^{**}$ (61 MHz)	2.07
6	B0919+06	238 ± 72	570 ± 171	3.91	$770 \pm 160^{**}$ (85 MHz)	0.25
7	B0943+10	133 ± 40	198 ± 60	1.78	$1290 \pm 350^{**}$ (61 MHz)	2.1
8	B0950+08	122 ± 37	284 ± 86	3.79	$2330 \pm 1620^{**}$ (102.5 MHz)	1.49
9	B1112+50	19 ± 6	25 ± 8	1.23	$60 \pm 14^*$ (102.5 MHz)	0.62
10	B1133+16	105 ± 32	283 ± 86	4.44	$1280 \pm 550^*$ (102.5 MHz)	1.07
11	B1237+25	16 ± 5	33 ± 10	3.24	$530 \pm 100^{**}$ (102.5 MHz)	1.97
12	B1508+55	35 ± 11	96 ± 29	4.52	$1280 \pm 500^*$ (102.5 MHz)	1.84
13	B1839+56	32 ± 10	89 ± 27	4.58	$120 \pm 50^{**}$ (102.5 MHz)	0.21
14	B1919+21	240 ± 73	490 ± 148	3.2	$2100 \pm 430^{**}$ (61 MHz)	1.63
15	B1929+10	50 ± 16	83 ± 25	2.27	$950 \pm 660^*$ (102.5 MHz)	1.73
				$m = 2.55$ $\sigma = 1.85$	$m = 1.14$ $\sigma = 0.77$	

*Malofeev et al. (2000).

**Izvekova et al. (1981).

if the S/N allows reliable measurement of the pulsar radiation in a band of 4 MHz, then the pulsar radio emission parameters are determined in the bands 23–27 and 18–22 MHz, which correspond to central frequencies of 25 and 20 MHz, respectively.

Errors in the flux measurements performed with large phased arrays such as UTR-2 include the following: (i) errors introduced by the electronic path between the antennas and the receivers, which can be estimated using an internal calibration system (including a reference noise generator), (ii) errors in dipole antenna responses (not covered by the calibration) and (iii) flux reflected and absorbed by the ground. The first error is no more than 1–2 per cent, thanks to the internal calibration. Imperfect knowledge of dipole parameters leads to an error of up to 10 per cent in flux measurements. The largest contribution is caused by our inaccurate knowledge of the conductivity of the soil. Despite monitoring of the ground conductivity and correcting our measurements for this parameter, this error may reach 15 per cent. The overall error in our flux density measurements thus does not exceed 30 per cent. The maximum error in spectral indices in Table 2, related to the quadratic combination of the above maximum error ~ 30 per cent in flux densities, is typically ± 1.8 .

For those pulsars that have an insufficient S/N in a bandwidth of 4 MHz, we have integrated the signal over the range 20–32 MHz (centre frequency of $\sqrt{20 \times 32} \sim 25.3$ MHz). In that case, errors (ii) and (iii) as well as the unknown pulsar flux-density spectrum lead to an estimated error of 50 per cent.

Flux densities of strong pulsars detected at two frequencies are shown in Table 2. The table also contains the spectral indices α_{20-25} (between frequencies 20 and 25 MHz) and $\alpha_{25-\nu_{\max}}$ (between 25 MHz and the frequency ν_{\max} at which the maximum flux density was measured) for those pulsars for which these data are known from the literature (Izvekova et al. 1981; Malofeev et al. 2000). ν_{\max} is given in the second row of the sixth column.

In Table 3, results on pulsars detected with a low S/N are given. Here, we integrate over the 20–32 MHz range and indicate the flux as well as the spectral index $\alpha_{25-\nu_{\max}}$.

Taking into account the small frequency spacing between 20 and 25 MHz and the above errors in measuring flux densities, the spectral index α_{20-25} should be considered with caution. However, even with this limited accuracy, one can note that the average value of the low-frequency spectral index of the 15 pulsars in Table 2 ($\langle \alpha_{20-25} \rangle = 2.55$) significantly exceeds the average value of the spectral index between decametre and metre waves ($\langle \alpha_{25-\nu_{\max}} \rangle \approx 1.1$). This may reveal the steepening of the spectral index in the decametre range, provided that measurements at ν_{\max} (especially the position of the maximum flux density) are reliable. Further studies with UTR-2 and LOFAR will help to clarify this issue. The average spectral index of strong pulsars in Table 2 ($\langle \alpha_{25-\nu_{\max}} \rangle \approx 1.1$) is smaller than that of weaker pulsars (≈ 1.4 , Table 3). i.e. the latter ones have a steeper spectrum from metre to decametre wavelengths, which naturally explains their smaller flux density at low frequencies.

Table 4 shows the upper limit of detection at 4σ for non-detected pulsars, with parameters $\Delta\nu = 4$ MHz, $\Delta t = 5400$ s, $(t_i/P) = 0.1$. In Section 4 we discuss the possibility of detecting the remaining pulsars from our sample.

3.3 Pulse width at the 50 per cent and 10 per cent levels and scattering time constant

On the basis of the accurate DM values in Table 1, we obtained average pulse shapes from which pulse widths at 50 per cent level (FWHM) and, whenever possible, at 10 per cent of the maximum intensity were determined (Table 5). Also, the scattering time constant at 25 MHz and the power-law exponent of the scattering variations between 25 and 1000 MHz (Manchester et al. 2005) were calculated. In the decametre range, the scattering time can be comparable to or even greater than the pulse width, even for nearby pulsars. Obviously, in this case it is difficult to separate the effects of scattering and intrinsic profile broadening versus frequency. The separation of these effects requires a specific approach as in Hassall et al. (2012), which is beyond the scope of this paper. In Table 5 we indicate the values of the pulse width at 50 per cent ($W_{0.5}$) and 10 per cent ($W_{0.1}$) levels, the scattering time constant at 25 MHz τ_{SC25} and the value of the power-law index $\alpha_{\text{SC25-1000}}$ obtained from the plots shown in Figs A1 and A2 and in the literature. These latter values are upper bounds because τ_{SC25} was determined by fitting the intensity decrease versus time in the pulse tail by a law $\propto e^{-t/\tau_{\text{SC25}}}$, assuming a rectangular shape for the pulse in emission. More precise values, taking into account a realistic pulse shape, will be obtained in the future (in preparation). Values of τ_{SC25} for four pulsars denoted by an asterisk in Table 5 were taken from Ulyanov & Zakharenko (2012), where this parameter was defined on the basis of records of

Table 3. Parameters of those pulsars detected with a low S/N; flux at 25 MHz and spectral indices α_{25-MW} for those pulsars for which these data are known from the literature.

N	Pulsar	Flux (mJy) (25 MHz)	Flux (mJy) (ν_{\max})	$\alpha_{25-\nu_{\max}}$
1	J0051+0423	32 ± 16	—	—
2	B0148-06	1.4 ± 1	$109 \pm 55^*$ (102.5 MHz)	3.09
3	B0320+39	29 ± 15	$230 \pm 70^*$ (102.5 MHz)	1.47
4	B0329+54	140 ± 71	$1050 \pm 210^{**}$ (102.5 MHz)	1.43
5	B0450+55	37 ± 19	$150 \pm 60^*$ (102.5 MHz)	0.99
6	J0927+23	8.5 ± 5	$30 \pm 13^*$ (102.5 MHz)	0.89
7	B0940+16	7.3 ± 4	$190 \pm 120^{**}$ (102.5 MHz)	2.31
8	J1238+21	19 ± 10	$60 \pm 22^*$ (102.5 MHz)	0.81
9	B1322+83	5.8 ± 3	$36 \pm 12^*$ (102.5 MHz)	1.29
10	B1530+27	19 ± 10	$94 \pm 44^*$ (102.5 MHz)	1.13
11	B1540-06	5.2 ± 3	$130 \pm 30^*$ (102.5 MHz)	2.28
12	B1604-00	5.0 ± 3	$330 \pm 70^{**}$ (102.5 MHz)	2.97
13	B1612+07	33 ± 17	$100 \pm 40^*$ (102.5 MHz)	0.79
14	B1633+24	25 ± 13	$50 \pm 15^*$ (102.5 MHz)	0.49
15	J1741+2758	14 ± 8	$30 \pm 10^*$ (102.5 MHz)	0.54
16	B1822-09	47 ± 24	$790 \pm 160^{**}$ (61 MHz)	3.16
17	J1851-0053	7.0 ± 4	—	—
18	J1908+0734	6.4 ± 4	—	—
19	B1944+17	27 ± 14	$150 \pm 90^{**}$ (102.5 MHz)	1.22
20	B1952+29	15 ± 8	—	—
21	B2016+28	71 ± 36	$260 \pm 100^*$ (102.5 MHz)	0.92
22	B2110+27	105 ± 53	$130 \pm 30^*$ (102.5 MHz)	0.15
23	J2307+2225	2.7 ± 2	$30 \pm 13^*$ (102.5 MHz)	1.71
24	B2310+42	21 ± 11	$110 \pm 90^*$ (102.5 MHz)	1.17
25	B2315+21	27 ± 14	$100 \pm 30^*$ (102.5 MHz)	0.93

$$m = 1.42$$

$$\sigma = 0.87$$

*Malofeev et al. (2000).

**Izvekova et al. (1981).

Table 4. Upper limits (at 4σ) of flux densities of non-detected pulsars.

N	Pulsar	Flux (mJy) (25 MHz)	N	Pulsar	Flux (mJy) (25 MHz)
1	J0006+1834	≤ 75	18	J1549+2113	≤ 90
2	J0137+1654	≤ 68	19	J1740+1000	≤ 130
3	J0152+0948	≤ 74	20	J1817-0743	≤ 210
4	B0301+19	≤ 66	21	J1832+0029	≤ 240
5	B0410+69	≤ 92	22	J1848+0647	≤ 210
6	J0459-0210	≤ 83	23	J1917+0834	≤ 180
7	B0609+37	≤ 81	24	B1916+14	≤ 160
8	B0656+14	≤ 85	25	J1918+1541	≤ 150
9	B0655+64	≤ 69	26	B1918+26	≤ 120
10	B0820+02	≤ 69	27	J2015+2524	≤ 120
11	B0917+63	≤ 59	28	B2020+28	≤ 125
12	J0943+22	≤ 44	29	B2021+51	≤ 106
13	J0947+27	≤ 43	30	J2151+2315	≤ 83
14	J1046+0304	≤ 78	31	J2215+1538	≤ 82
15	J1246+22	≤ 58	32	J2248-0101	≤ 81
16	J1313+0931	≤ 100	33	J2253+1516	≤ 78
17	J1503+2111	≤ 87	34	J2346-0609	≤ 95

individual pulses with high time resolution. They were not considered in the calculation of the mean value of $\alpha_{\text{SC25-1000}}$.

The obtained average value of $\alpha_{\text{SC25-1000}}$ (4.01) and its standard deviation (0.24) are close to those obtained by Kuzmin, Losovskii & Lapaev (2007) (4.1 ± 0.3). However, estimates of the power-law index $\alpha_{\text{SC25-1000}}$ for many pulsars in Table 5 appear to be significantly lower than the index corresponding to a Kolmogorov distribution (4.4).

4 DISCUSSION

Not only the number of detected pulsars but also their observed peak S/N values (after accurate DM determination) show promising prospects in searching for pulsed and transient sources in the decametre range. Thus, we hope to discover periodic radio sources as well as aperiodic radio emissions.

4.1 Fraction of pulsars available for detection in the decametre range

The efficiency of the decametre survey of pulsed sources at UTR-2 depends directly on the relative fraction of pulsars available for observations at low frequencies.

The sensitivity of the survey is not the same for different sky regions. It depends first on the zenith angle of the source, and thus on the effective area of the telescope, and secondly on the Galactic background in the selected direction. Fig. 6 shows the 4σ upper limits (see Table 4) corresponding to non-detected pulsars as a function of hour angle (upper panel) and declination (right panel). The area close to the Galactic Centre (RA=17h45m) is clearly distinguishable. Here, both the effect of high temperature of the Galactic background and low δ of sources reduce the sensitivity simultaneously. In the anticentre direction, the impact of intense galactic noise is partially compensated for by the small zenith angles of the pulsars in that area observed from UTR-2. Fig. 6 also gives the ratio $A_e/A_{e\max}$. The number of non-detected pulsars does not depend strictly on the zenith angle. The left lower panel shows the comparison between the coordinates of the detected (crosses) and non-detected pulsars (diamonds with normalized values of the

Table 5. Pulse width $W_{0.5}$, $W_{0.1}$ at the level of 0.5 and 0.1 of the maximum intensity at frequencies of 20 and 25 MHz, with the characteristic scattering time in the decametre range τ_{SC25} and the power-law index of the scattering parameters at these frequencies $\alpha_{SC25-1000}$.

<i>N</i>	Pulsar	$\nu = 25$ MHz		$\nu = 20$ MHz		τ_{SC} (25 MHz)	α_{SC} (25–1000 MHz)
		$W_{0.5}$	$W_{0.1}$	$W_{0.5}$	$W_{0.1}$		
		(ms)	(ms)	(ms)	(ms)	(ms)	
1	B0031–07	79(10)	175(20)	103(10)	222(20)	44(10)	4.3
2	0051+0423	99(20)	191(40)	87(20)	127(40)	48(20)	–
3	B0053+47	111(10)	211(20)	115(10)	290(20)	55(10)	–
4	B0148–06	–	–	–	–	–	–
5	B0320+39	393(20)	703(40)	–	–	200(20)	3.91
6	B0329+54	246(20)	470(40)	–	–	145(20)	3.97
7	B0450+55	87(20)	195(40)	–	–	52(20)	3.93
8	B0809+74	70	151	75	151	2.5(5)*	–
9	B0823+26	97(10)	146(20)	–	–	37(10)	3.84
10	B0834+06	80(10)	180(20)	122(10)	246(20)	60(10)	4.25
11	B0919+06	151(10)	286(20)	183(10)	266(20)	60(10)	3.56
12	J0927+23	234(20)	532(40)	342(20)	592(40)	150(20)	–
13	B0940+16	258(20)	377(40)	191(20)	437(40)	60(20)	–
14	B0943+10	71	153	112	226	12(2)*	–
15	B0950+08	39	67	44	75	1(0.05)*	–
16	B1112+50	131(10)	246(20)	179(10)	457(20)	65(10)	4.18
17	B1133+16	81	157	96	181	6.5(5)*	–
18	J1238+21	147(20)	342(40)	222(20)	449(40)	72(20)	–
19	B1237+25	49(10)	159(20)	62(10)	192(20)	14(10)	4.0
20	B1322+83	36(20)	76(40)	–	–	15(10)	–
21	B1508+55	142(10)	338(20)	203(20)	280(20)	125(10)	3.79
22	B1530+27	135(20)	203(40)	–	–	20(10)	4.05
23	B1540–06	75(20)	132(40)	–	–	30(20)	4.06
24	B1604–00	61(20)	126(40)	100(20)	172(40)	56(20)	4.41
25	B1612+07	361(20)	616(40)	–	–	180(20)	4.38
26	B1633+24	132(20)	–	168(20)	323(40)	68(20)	–
27	J1741+2758	–	–	–	–	–	–
28	B1822–09	–	–	–	–	–	–
29	B1839+56	196(10)	409(20)	356(10)	516(20)	110(10)	3.76
30	J1851–0053	–	–	–	–	–	–
31	J1908+0734	52(20)	155(40)	–	–	30(20)	–
32	B1919+21	54(10)	107(20)	84(10)	156(20)	22(10)	3.95
33	B1929+10	31(10)	60(20)	37(10)	60(20)	–	–
34	B1944+17	73(20)	105(40)	–	–	20(10)	3.51
35	B1952+29	15(10)	–	–	–	–	–
36	B2016+28	99(20)	254(40)	–	–	70(20)	3.9
37	B2110+27	265(20)	354(40)	249(20)	452(40)	52(20)	3.92
38	J2307+2225	–	–	–	–	26(20)	–
39	B2310+42	95(20)	196(40)	–	–	40(20)	–
40	B2315+21	130(20)	294(40)	–	–	72(20)	4.18

$m = 4.01$
 $\sigma = 0.24$

*Ulyanov & Zakharenko (2012).

upper limit of detection, as also plotted in the upper panel). Values in Fig. 6 were normalized by the 4σ level for PSR B0809+74 (dashed line). Fig. 6 shows that the sensitivity achieved by the observations for almost all non-detected pulsars is lower than that for PSR B0809+74 by 1.4–4.5 times. An increase in sensitivity can be achieved by increasing the integration time (currently 90 min to 6–8 h), which will allow us to reduce the detection threshold for sources of periodic pulsed radiation by a factor of 1.5–2.5. In this case, the sensitivity for more than 25 pulsars of our sample would be better than the sensitivity reached for PSR B0809+74 after 90 min integration.

To analyse the possibility of detecting more pulsars by increasing the sensitivity, we have plotted a histogram (Fig. 7) of the 400-MHz fluxes (taken from Manchester et al. 2005) of the pulsars that we detected. The number of pulsars detected in the decametre range (solid line) and all pulsars from the sample (dash-dotted line) are

displayed on a linear scale in the left panel of Fig. 7 and on a logarithmic scale in the right panel.

Of course, the flux at 400 MHz cannot be directly related to the flux at 25 MHz because of different spectral indices and propagation effects in the interstellar medium. This is illustrated by the non-detection of the pulsar B2021+51, which nevertheless has a high flux density at 400 MHz (77 mJy). In spite of these particular cases, there is a clear relation between the fraction of detected pulsars and their flux (lower panel of Fig. 7). A sensitivity increase by one step of the histogram ($10^{0.5}$ times) approximately doubles the number of detected pulsars at low flux densities. Thus our expected sensitivity increase by a factor of 1.5–2.5 should allow us to detect about 10–15 pulsars from the remaining 34 non-detected targets of our initial sample.

The second factor that significantly reduces the amount of detected pulsars is interference. Numerous occurrences of low-intensity broad-band and narrow-band RFI are visible in the ‘rotational phase–dispersion measure’ plane, after dedispersion, pulse accumulation and integration in frequency, as lines with various slopes and intensities. Fig. 8 illustrates the impact of interference on the attempt to detect PSR J2215+1538. An increase in intensity is visible both at a DM close to that given in Manchester et al. (2005) and at a DM lower by 0.3 pc cm^{-3} . Moreover, the region of maximum intensity at higher DMs is non-homogeneous. This may be explained by the influence of weak broad-band interference, which has not been well removed by our cleaning procedures. Usually, when searching for the true DM of a pulsar observed in polluted conditions, we split the spectrum into different frequency bands. If the DM found in different bands (as in Fig. 3) is the same for all data sets, we regard it as certain (as it is the case, for example, for PSRs B1540–06, J1908+0734 and B1944+17 in Fig. 2a). For PSR J2215+1538, as well as a dozen other pulsars, there are two or more intensity maxima in the ‘rotational phase–dispersion measure’ plane for different frequency bands. We cannot decide between these various maxima from the presently available data. We therefore cannot conclude a reliable detection of these pulsars in the absence of additional measurements. Observations in more favourable interference conditions (the current observations were partially taken in the daytime, under non-optimal interference conditions) will probably allow us to detect a few more pulsars from our sample.

At a result of the present study, the fraction of pulsars with $DM < 30 \text{ pc cm}^{-3}$ detected in the decametre range is ≈ 55 per cent. With increased observing time and/or improved interference elimination, this value should rise up to 60–80 per cent.

Besides observing all sources in our sample, we have conducted several observations of pulsars with $DM > 30 \text{ pc cm}^{-3}$. Fig. 9 shows the successful detection of PSR B0525+21 with a DM $\approx 50.9 \text{ pc cm}^{-3}$. The pulsar was observed during the daytime (local time in the range 16:50–18:20) and the observation was affected by powerful interference (cf. Fig. 3). The upper panel of Fig. 9 shows the normalized dynamic spectrum of the observation. The data contain a strong signal from the Crab nebula, entering through the telescope’s side lobes.

Further processing was complicated not only by scintillation but also by the presence of broad-band noise in the range 27.5–30.5 MHz. However, in spite of the interference and the high temperature of the Galactic background in that field, the dual-peak profile of PSR B0525+21 can be recognized both in the average profile (lower left panel) and in the grey-scale ‘rotational phase–dispersion measure’ image (lower right panel). Obviously, the normalization by off-pulse radiation, which is heavily affected by the interference

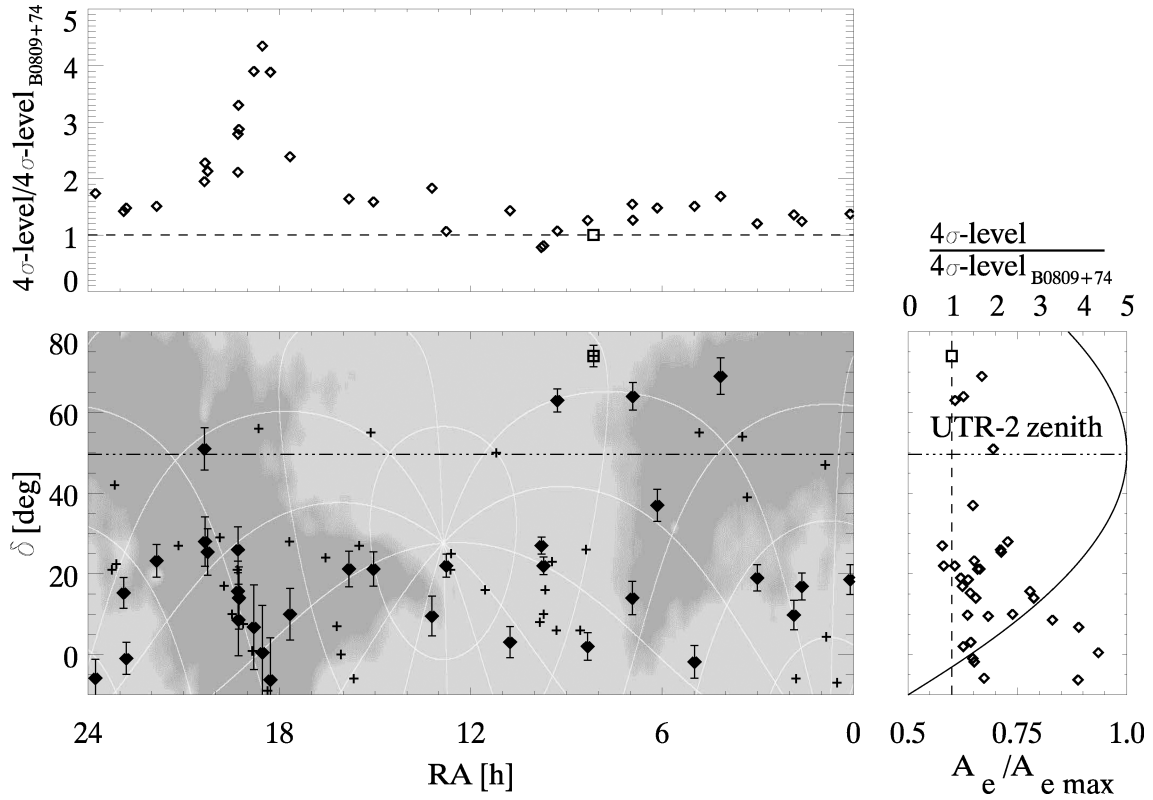


Figure 6. Upper limit on the flux density of non-detected pulsars (duty cycle 0.1, $\Delta\nu = 4$ MHz) as a function of hour angle (upper panel) and declination (right panel). The left lower panel shows, for comparison, the coordinates of the detected (crosses) and non-detected pulsars (diamonds with normalized values of the 4σ detection limit). Positions of the pulsars are overlapped on the northern sky map at 20 MHz (Sidorchuk et al. 2008). The peak in the upper panel corresponds approximately to the direction of the Galactic Centre. Detection limits were normalized by the 4σ level for PSR B0809+74 (open square and dashed line).

and probably by scintillations, gives an underestimated S/N value in this case. Flux estimates obtained with formula (2) are significantly underestimated as well. The same can be said about a few other pulsars, for which the off-pulse part of the period is also distorted by the influence of low-intensity RFI (Fig. 2a). In addition, due to the impact of interference, the fraction of excluded samples (narrow-band frequency channels and/or selected time intervals) was about 50 percent for the case of PSR B0525+21. For this reason, the accuracy in the DM was much lower than for other pulsars (± 0.1 pc cm $^{-3}$). Moreover, the observational parameters ($\Delta t = 8$ ms, $\Delta\nu = 4$ kHz) and the incoherent method of dispersion compensation resulted in a significant ‘smearing’ of the signal in the low-frequency channels (up to 170 ms, which is comparable to the broadening due to scattering). However, for the observation of more distant sources, observation parameters and methods of dispersion compensation can be optimized. The usage of the upper part of the operating frequency range, where the dispersion delay is smaller, makes it possible to detect more distant pulsars with only a small loss in sensitivity.

The detection of PSR B0525+21 indicates the high potential of the telescope and our processing algorithms, which can recover weak signals in the strong interference background of daytime observations. The estimation of the distance of PSR B0525+21 (Cordes & Lazio 2002) is ≈ 1.6 kpc and that of PSR B0138+59 (which we detected with a DM of 34.98 ± 0.02 pc cm $^{-3}$) is ≈ 2.2 kpc, PSR J1238+21 ≈ 2.2 kpc, PSR J1741+2758 ≈ 1.7 kpc,

PSR B1839+56 ≈ 1.7 kpc and PSR B2110+27 ≈ 2.0 kpc. For this reason, we believe that, even though the fraction of detectable pulsars decreases at low frequencies, the detection volume for pulsars can still be important in the decametre wavelength range.

4.2 Impact of scattering in the ISM on the number of detected sources of pulsed radiation at low frequencies

Analysis of the data in the catalogue (Manchester et al. 2005) shows that, up to values of DM 60–70 pc cm $^{-3}$, pulsars have a scattering time constant that still allows their detection at low frequencies. For those pulsars, Fig. 10 shows the scattering time constant values normalized by the pulse period as a function of the DM. The rectangle on the picture denotes PSR B1822–09, successfully detected during our observations. We see that only 15–20 per cent of all pulsars with DM 0–70 pc cm $^{-3}$ have a scattering time constant that is noticeably higher than that of PSR B1822–09.

In addition, our measurements (see Section 3), even if we consider them upper estimates, show that for a significant number of pulsars the exponent that describes the increase of characteristic scattering time is somewhat less than 4.4. This will hopefully allow us to detect more pulsars and transient sources in the decametre range. For a more accurate separation of the effects of pulse broadening and scattering, joint observations of LOFAR and UTR-2 covering the range 10–90 MHz are required.

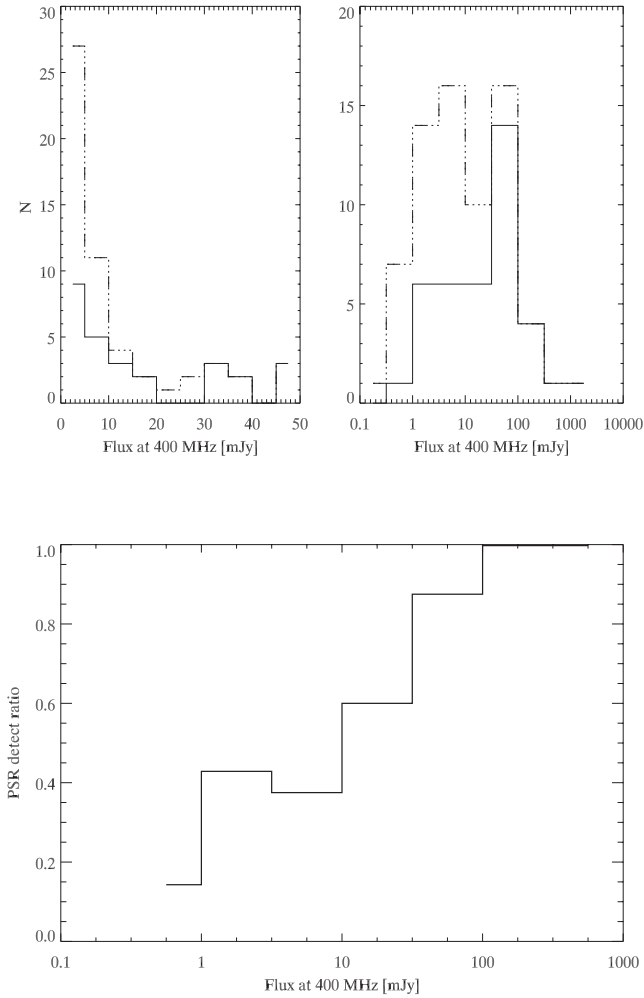


Figure 7. Distribution histograms of detected pulsars (solid line) and of the full sample (dashed line) on a linear scale (left panel) and a logarithmic one (right panel). The bottom panel shows the ratio of the detected pulsars to the entire number in the sample.

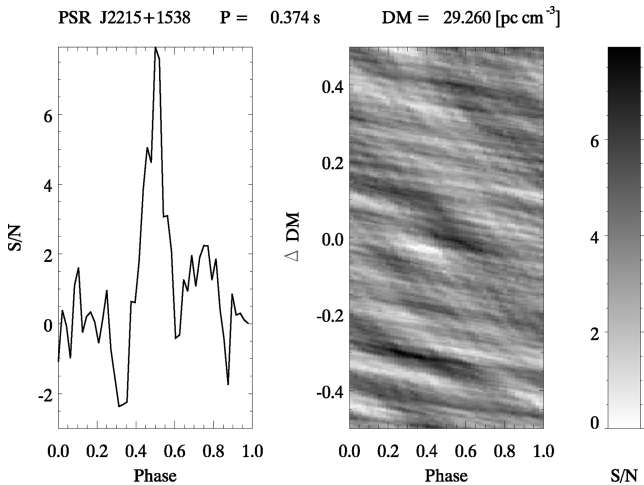


Figure 8. Impact of interference while attempting to detect the pulsar J2215+1538. Characteristic intensity increases are seen for both a DM close to the one given in Manchester et al. (2005) and a DM lower by 0.3 pc cm^{-3} .

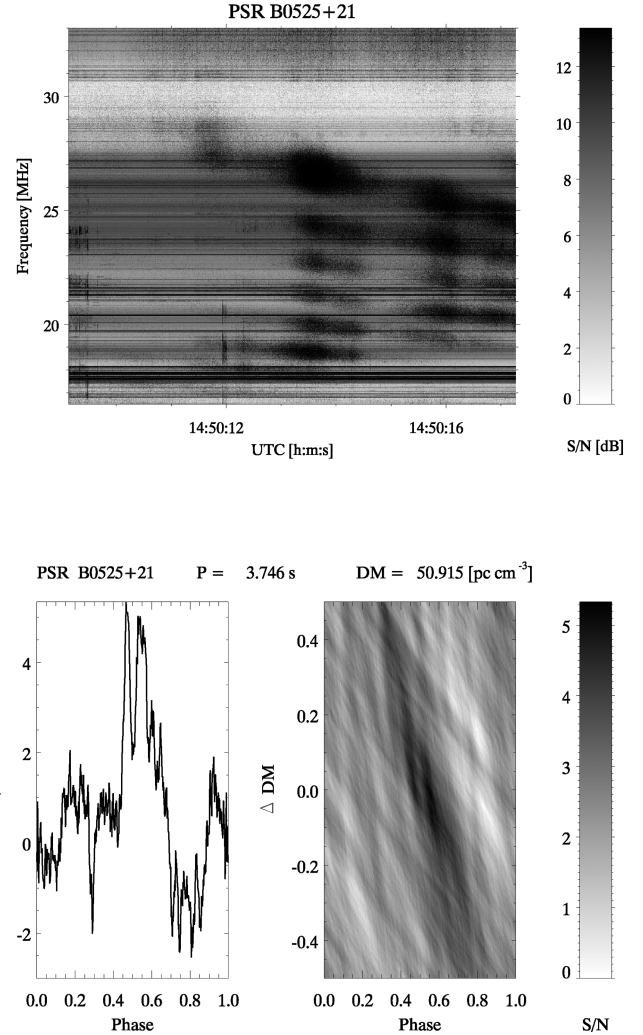


Figure 9. Normalized dynamic spectrum of the observation of PSR B0525+21 (upper panel). The data contain a strong signal from the Crab nebula, entering through the telescope's side lobes. The lower panel shows the result of the successful detection of the pulsar at $\text{DM} \approx 50.9 \text{ pc cm}^{-3}$.

4.3 On the possibility of detecting new sources due to growth of the beaming fraction

The main factor that could lead to an increase in the number of detected pulsars in the decametre range is the intrinsic widening of the pulse profile (Cordes 1978; Thorsett 1991). As mentioned above, Cordes (1978) found a pulse width $\propto \nu^{-0.25}$. A similar relation for pulse component separation was obtained in Thorsett (1991). The distance between the components Θ is described by the formula

$$\Theta = A f^{-\alpha_c} + \Theta_0, \quad (4)$$

where A , α_c and Θ_0 are parameters specific for each pulsar. For pulsars listed by Thorsett (1991), the exponent in this equation is $0.34 \leq \alpha_c \leq 1.08$.

Intrinsic pulse widening was extrapolated for frequencies of 25 and 100 MHz using both the parameters and pulsars from Thorsett (1991). In Fig. 11 these data are indicated by bold crosses. We calculated that the relative pulse widening between 25 and 100 MHz is in the range 1.3–2.6.

Using the data from Table 5, we calculated the values of pulse widening for pulsars detected with a sufficient S/N (Table 2) for

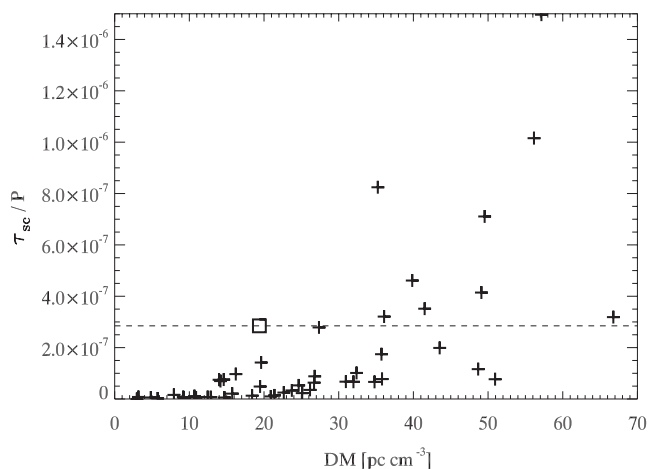


Figure 10. Scattering time constant values at 1 GHz (Manchester et al. 2005) normalized by the period of each pulsar as a function of the DM. The rectangle denotes the pulsar B1822-09, successfully detected during our observations. Only 15–20 per cent of all pulsars have a scattering time constant high enough potentially to hinder their detection at low frequencies.

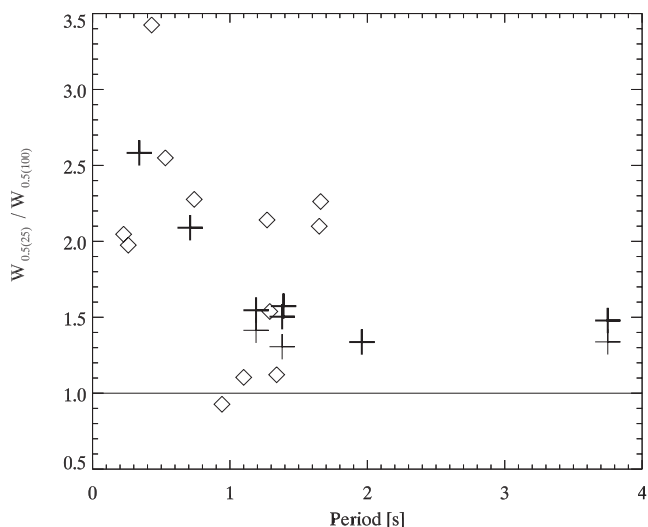


Figure 11. Relative expansion of the FWHM profile between frequencies 25 and 100 MHz as a function of period. Bold crosses are extrapolated from the parameters obtained in Thorsett (1991) for pulsars B0301+19, B0329+54, B0525+21, B1133+16, B1237+25, B2020+28 and B2045-16. Thin crosses correspond to pulsars in common in Thorsett (1991) and in the present study (B0525+21, B1133+16, B1237+25), while diamonds denote the other pulsars from our study.

the same frequencies 25 and 100 MHz. To do this, we estimated and subtracted the broadening due to scattering in the ISM from the $W_{0.5}$ width. As we consider that upper estimates were obtained for τ_{sc} , the corrected values of $W_{0.5}$ might be underestimated. In Fig. 11 these estimates from UTR-2 measurements only are denoted by diamonds and thin crosses. The latter correspond to pulsars also listed in Thorsett (1991) (PSRs B0525+21, B1133+16 and B1237+25), whereas diamonds denote the other pulsars from our study. Our estimates for the three coincident pulsars are somewhat lower (by 5–15 per cent) than the relative width obtained in Thorsett (1991), consistent with our assumptions about underestimating the corrected pulse width at low frequencies. However, for almost all

pulsars we obtain a substantial pulse widening (on average a factor of 1.8, with a standard deviation of 0.7).

Except for a few rare cases, for which the pulse profile becomes narrower towards low frequencies (see Fig. 11), most profiles broaden towards low frequencies, which suggests that the number of visible pulsed and transient sources should increase at low frequencies. In the present study, 40 pulsars with DM 0–30 pc cm^{-3} , $\delta = -10$ – 90° and period >0.1 s were detected. We confirmed that the beaming fraction increases at low frequencies (Fig. 11), so at lower frequencies the pulsar beam will more likely cross Earth. If we estimate that fraction as 1.5 (the beam at 25 MHz is 50 per cent wider than at 100 MHz), we can expect the detection of nearly 20 new pulsed sources that are not visible at higher frequencies.

5 CONCLUSIONS

From the full sample of sources with declination above -10° , period longer than 0.1 s and DM less than 30 pc cm^{-3} , we have detected at UTR-2 the radio emission of 40 pulsars, of which 30 have never been detected in the decametre range previously. For most of the detected pulsars, the DM values have been considerably refined and the values of the flux density at 25 ± 2 and 20 ± 2 MHz (or in the band 20–32 MHz) have been obtained for the first time. Spectral indices α_{20-25} and $\alpha_{25-\nu_{\max}}$ have been calculated for those pulsars, for which the flux data at metre wavelengths are taken from the literature. The pulse width at 50 per cent and 10 per cent levels relative to the maximum intensity has been measured. We have estimated for the first time the high detection fraction in the decametre range (~ 55 per cent) and we have demonstrated that the characteristics of pulsar radio emission can be determined with high accuracy. On average, the values of $\alpha_{SC25-1000}$ are smaller than 4.4, which favours the discovery of pulsars with DMs up to 70 pc cm^{-3} . As a confirmation, the pulsars B0138+59 and B0525+21 have been detected with DM ≈ 34.9 pc cm^{-3} and ≈ 50.9 pc cm^{-3} , respectively. An upper limit for $\alpha_{SC25-1000}$ (the spectral index of the scattering time-scale τ_{SC25}) has been obtained. Values of the intrinsic widening of the pulsar profiles at low frequencies have been estimated, which agree well with the few known from the literature. This widening of the average pulse profile of most pulsars at low frequencies provides unique information about the nearest sources of repeating and, in particular, transient radiation (RRAT, giant pulses of pulsars). The present work has shown for the first time that in the decametre range the detection and study of the majority of nearby slow pulsars is possible and that we can expect the detection of new sources of transient and pulsed radiation, most of which cannot be observed at higher frequencies. We take this as motivation to conduct a full survey of the northern sky at low frequencies, aimed at searching for pulsars and transient sources in the Galactic neighbourhood. Such a survey is both useful, required and achievable.

ACKNOWLEDGEMENTS

This work was partly supported by ANR programme NT05-1-42530 ‘Radio-Exopla’ and pursued in the frame of the NASU-CNRS PICS program ‘Development of LF radioastronomy with ultrahigh sensitivity and resolution’ (Grant 1.33.11). This work is also supported by the National Academy of Sciences of Ukraine and the Russian Foundation for Basic Research (Ukrainian–Russian Project 2012). We thank the authors of the ATNF Pulsar Catalogue (<http://www.atnf.csiro.au/people/pulsar/psrcat/>; Manchester et al. 2005). We thank the referee for some very useful comments.

REFERENCES

- Abranin E. P., Bruck Yu. M., Zakharenko V. V., Konovalenko A. A., 2001, *Experimental Astron.*, 11, 85
- Backer D. C., Hama S., Hook S. V., Foster R. S., 1993, *ApJ*, 404, 636
- Bhat R. N. D. et al., 2007, *ApJ*, 665, 618
- Braude S. Ya., Megn A. V., Sodin L. G., 1978, *Antennas*, Vol. 26. *Sviaz'*, Moscow, p. 3
- Braude S. Ya., Rashkovsky S. L., Sidorchuk K. M., Sidorchuk M. A., Sokolov K. P., Sharykin N. K., Zakharenko S. M., 2002, *Ap&SS*, 280, 235
- Bruck Yu., 1970, *Izv. Vuzov Radiophysica*, 13, 1814
- Bruck Yu., 1987, *Aust. J. Phys.*, 40, 861
- Bruck Yu., Ustimenko B., 1973, *Nat*, 242, 58
- Bruck Yu., Ustimenko B., 1976, *Nat*, 260, 766
- Bruck Yu., Ulyanov O., Ustimenko B., 1986, *Sov. Astron. J.*, 63, 970
- Caswell J. L., 1976, *MNRAS*, 177, 601
- Cordes J. M., 1978, *ApJ*, 222, 1006
- Cordes J. M., Lazio T. J. W., 2002, preprint (astro-ph/0207156)
- Cordes J. M., McLaughlin M. A., 2003, *ApJ*, 596, 1142
- Deshpande A., Radhakrishnan V., 1992, *JA&A*, 13, 151
- Deshpande A. A., Radhakrishnan V., 1994, *JA&A*, 15, 329
- Diehl R. et al., 2006, *Nat*, 439, 45
- Ellis G. R. A., 1982, *Aust. J. Phys.*, 35, 91
- Hassall T. E. et al., 2012, *A&A*, 543, A66
- Hewish A., Bell S. J., Pilkington J. D. H., Scott P. F., Collins R. A., 1968, *Nat*, 217, 709
- Hobbs G., Lyne A. G., Kramer M., Martin C. E., Jordan C., 2004, *MNRAS*, 353, 1311
- Izvekova V. A., Kuzmin A. D., Malofeev V. M., Shitov Iu. P., 1981, *Ap&SS*, 78, 45
- Karuppusamy R., Stappers B. W., Serylak M., 2011, *A&A*, 525, A55
- Keane E. F., Kramer M., 2008, *MNRAS*, 391, 2009
- Kondratiev V. I., McLaughlin M. A., Lorimer D. R., Burgay M., Possenti A., Turolla R., Popov S. B., Zane S., 2009, *ApJ*, 702, 692
- Konovalenko A. A. et al., 2011, in Rucker H. O., Kurth W. S., Louarn P., Fischer G., eds, *Planetary Radio Emissions VII*. Austrian Academy of Sciences Press, Vienna, p. 521
- Kozhin R., Vynogradov V., Vavriv D., 2007, in Kostenko A., Nosich A., Yakovenko V., eds, *The Sixth International Kharkov Symposium on Physics and Engineering of Microwaves, Millimeter and Submillimeter Waves and Workshop on Terahertz Technologies, MSMW'07*, Kharkiv, Ukraine, p. 736
- Kuzmin A. D., Losovskii B. Ya., Lapaev K. A., 2007, *Astron. Rep.*, 51, 615
- Lecacheux A., Rosolen C., Clerc V., Kleweein P., Rucker H. O., Boudjada M., van Driel W., 1998, in Phillips T. G., ed., *Proc. SPIE Vol. 3357*, Advanced Technology MMW, Radio, and Terahertz Telescopes. SPIE, Bellingham, p. 533
- Malofeev V. M., Malov O. I., Shchegoleva N. V., 2000, *Astron. Rep.*, 44, 436
- Malofeev V. M., Malov O. I., Teplykh D. A., 2005, *Ap&SS*, 308, 211
- Manchester R. N., Hobbs G. B., Teoh A., Hobbs M., 2005, *AJ*, 129, 1993
- Maron O., Kijak J., Kramer M., Wielebinski R., 2000, *A&AS*, 147, 195
- McLaughlin M. A. et al., 2006, *Nat*, 439, 817
- Milogradov-Turin J., Smith F. G., 1973, *MNRAS*, 161, 269
- Phillips J. A., Wolszczan A., 1989, *ApJ*, 344, L69
- Phillips J. A., Wolszczan A., 1992, *ApJ*, 385, 273
- Popov M. V. et al., 2006, *Astron. Rep.*, 50, 562
- Reyes F., Carr T. D., Oliver J. P., May J., Bitran M., Aparici J., 1981, *Rev. Mex. Astron. Astrofis.*, 6, 219
- Roger R. S., Costain C. H., Landecker T. L., Swerdlyk C. M., 1999, *A&AS*, 137, 7
- Ryabov V. B., Vavriv D. M., Zarka P., Ryabov B. P., Kozhin R., Vinogradov V. V., Denis L., 2010, *A&A*, 510, A16
- Sidorchuk M. A., Ulyanov O. M., Shepelev V. A., Mukha D. V., Brazhenko A. I., Vashchishin R. V., Frantzenenko A. V., 2008, *Scientific Workshop – Astrophysics with E-LOFAR*, available at: http://www.hs.uni-hamburg.de/DE/Ins/Lofar/lofar_workshop/poster_abstracts.html
- Stappers B. W. et al., 2011, *A&A*, 530, 80
- Taylor J. H., Manchester R. N., Lyne A. G., 1993, *ApJS*, 88, 529
- Thorsett S., 1991, *ApJ*, 377, 263
- Ulyanov O., Zakharenko V., 2012, *Astron. Rep.*, 56, 417
- Ulyanov O. M., Zakharenko V. V., Konovalenko A. A., Lecacheux A., Rosole C., Rucker H. O., 2006, *Radiofizika and Radioastronomia*, 11, 113
- Ulyanov O. M., Deshpande A., Zakharenko V. V., Asgekar A., Shankar U., 2007, *Radiofizika and Radioastronomia*, 12, 5
- Ulyanov O., Zakharenko V., Bruck Yu., 2008, *AZh*, 85, 1
- Zakharenko V. V., Nikolaenko V. S., Ulyanov O. M., Motiyenko R. A., 2007, 12, 233
- Zakharenko V., Markova A., Vasylieva I., 2011, *Radio Phys. Radio Astron.*, 2, 15

APPENDIX A: PULSAR PROFILES

Average profiles of 15 pulsars with high S/N (Fig. A1) over bands 23–27 MHz (bold curve) and 18–22 MHz (thin curve) and average profiles of 25 pulsars with low S/N (Fig. A2) over the band 20–32 MHz (or 16.5–33.0 MHz for PSRs B0148–06, J1238+21, B0940+16 and B1822–09), along with grey-scale images of the ‘rotational phase–dispersion measure’ plane for each pulsar over the band 16.5–33.0 MHz (both Figs A1 and A2).

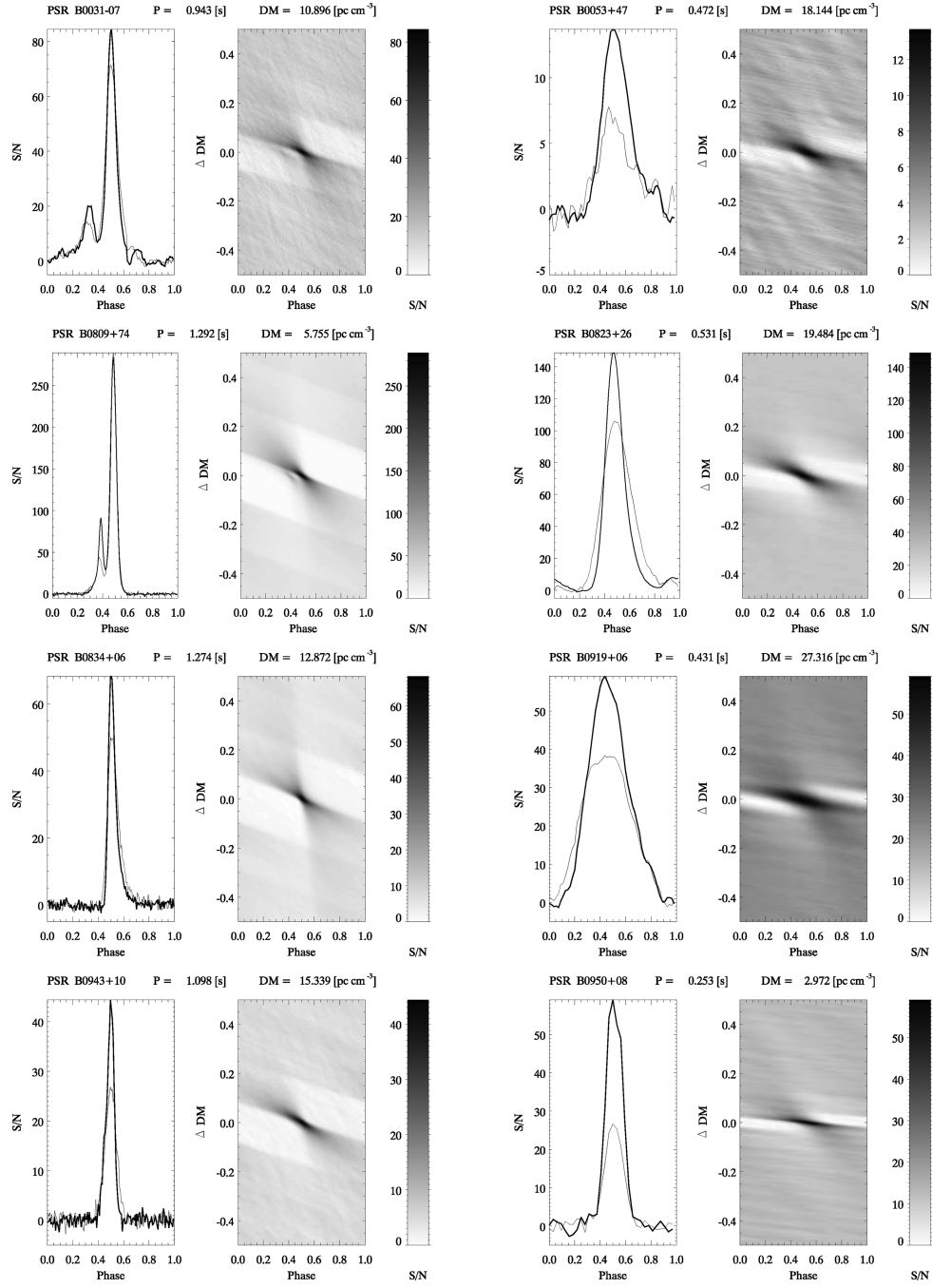


Figure A1. Average profiles of 15 pulsars with high S/N over the bands 23–27 MHz (bold curve) and 18–22 MHz (thin curve).

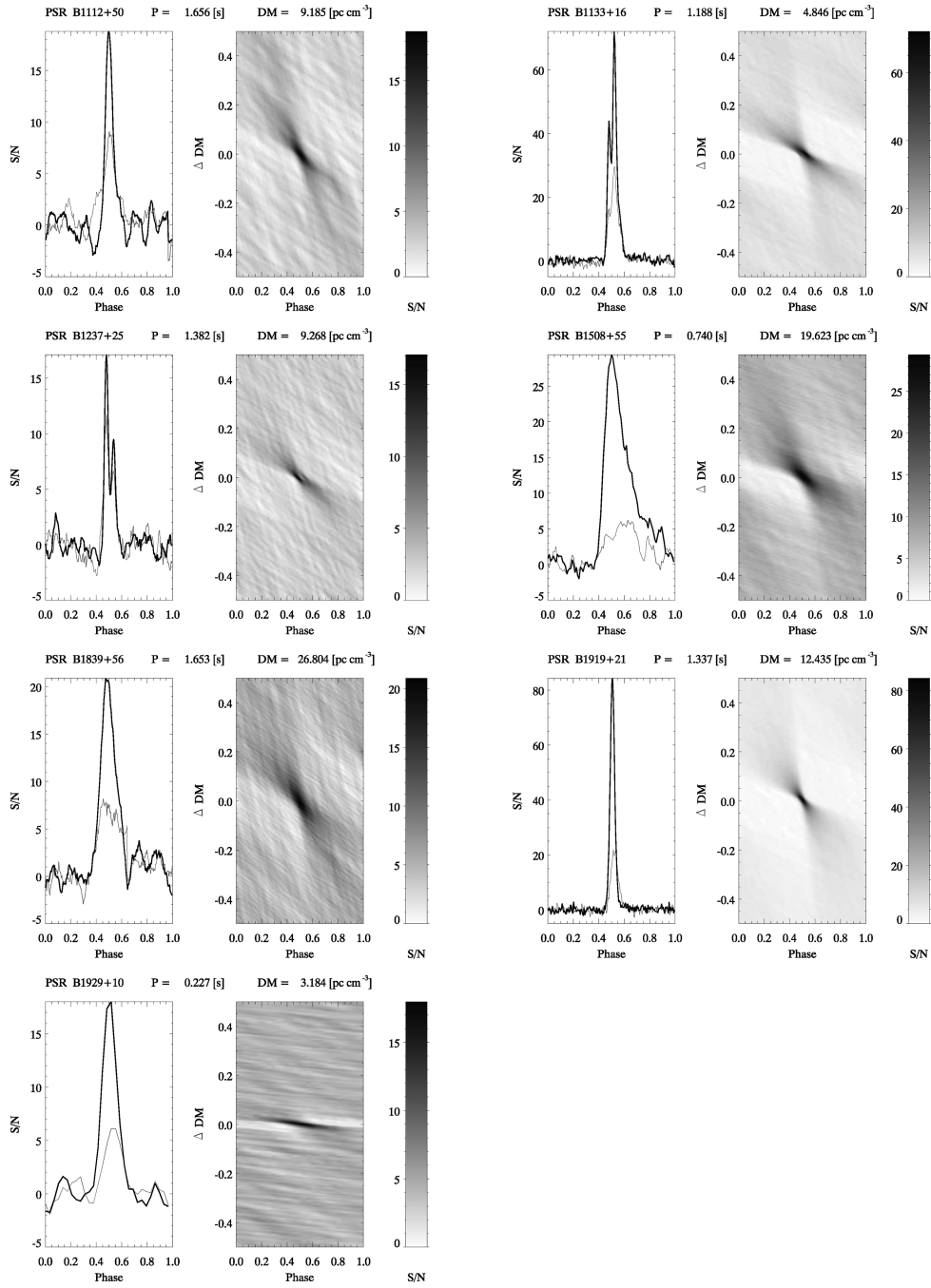


Figure A1 – continued

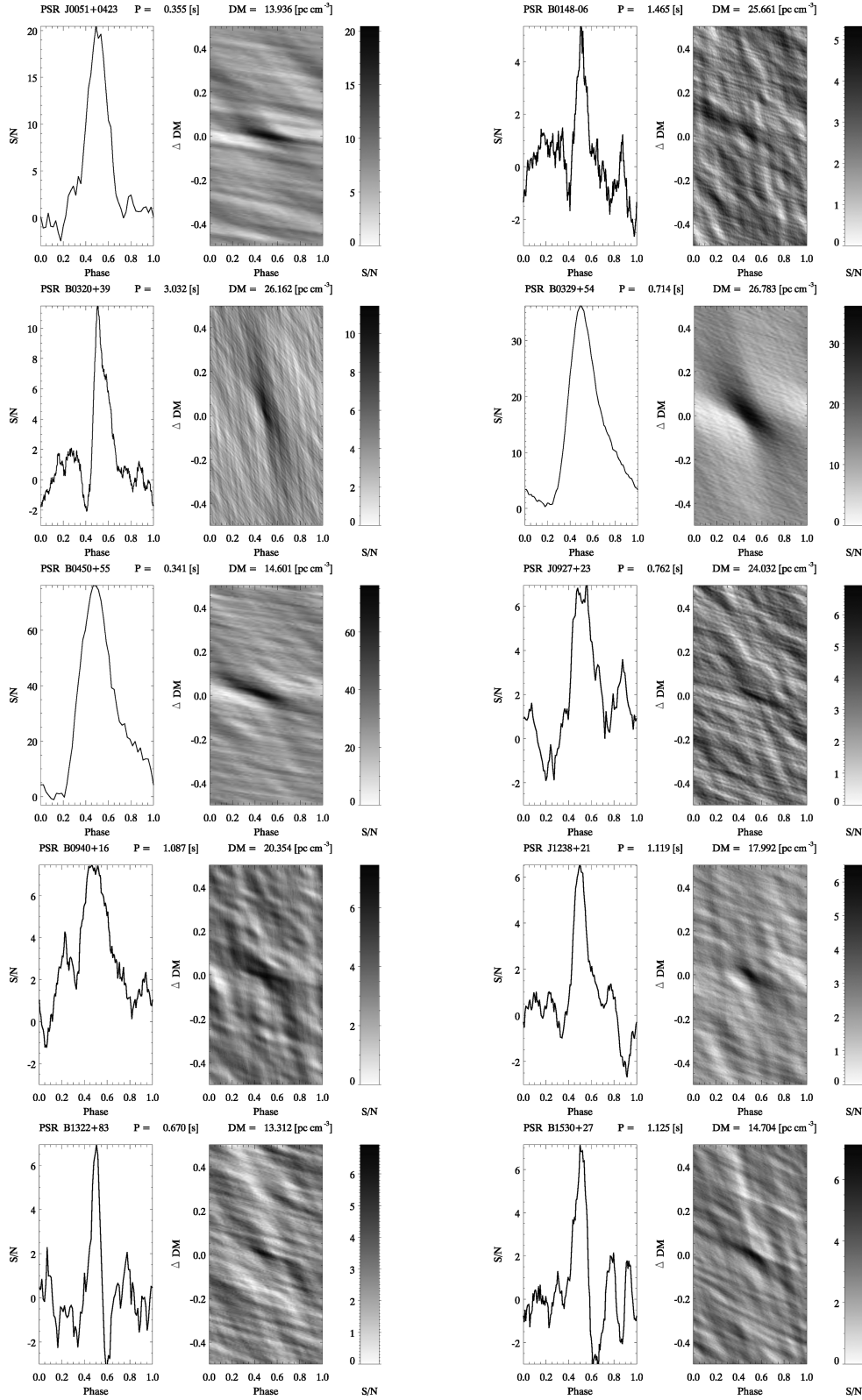
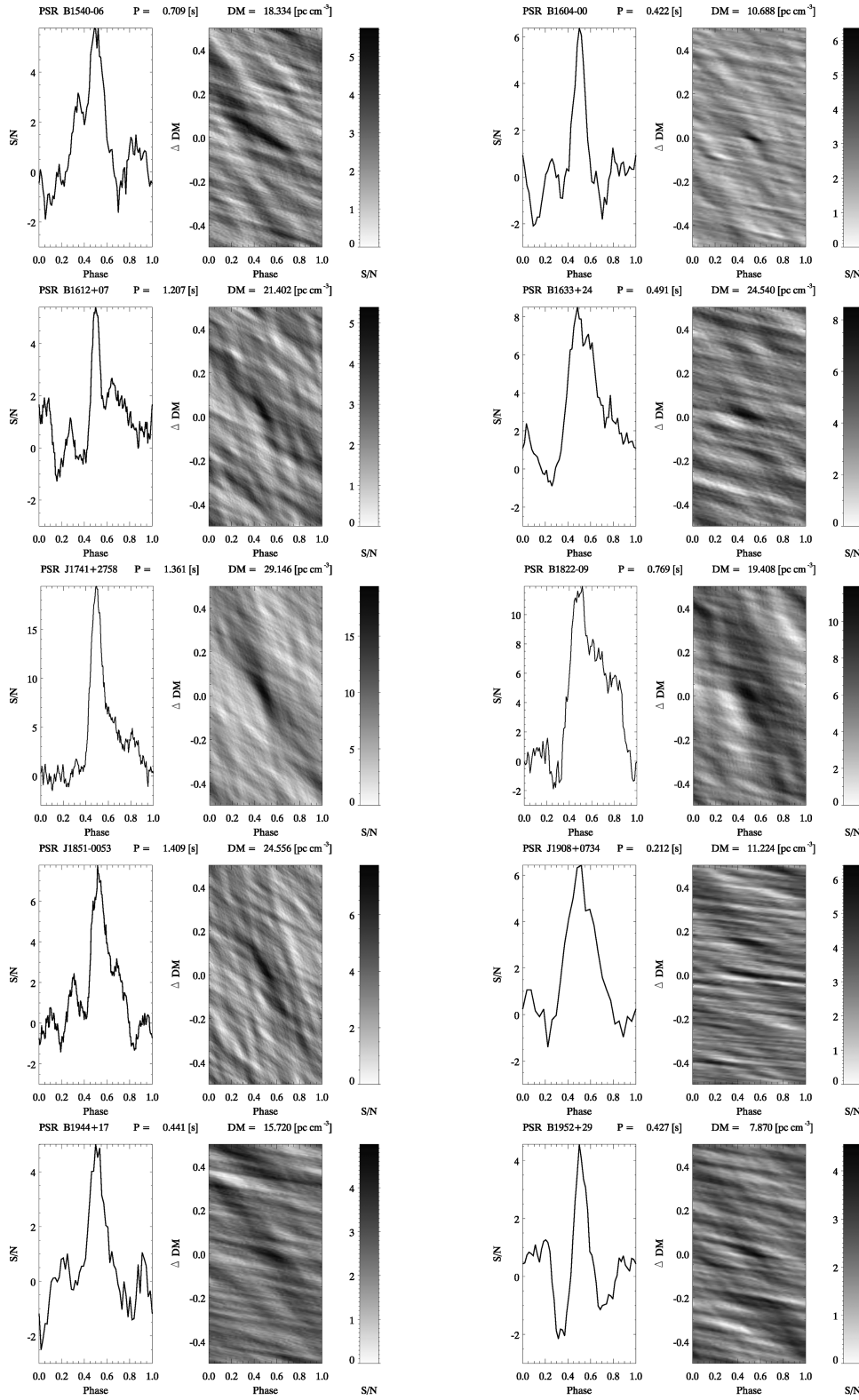


Figure A2. Average profiles of 25 pulsars with low S/N over the band 20–32 MHz (or 16.5–33.0 MHz for PSRs B0148–06, J1238+21, B0940+16 and B1822–09).

Figure A2 – *continued*

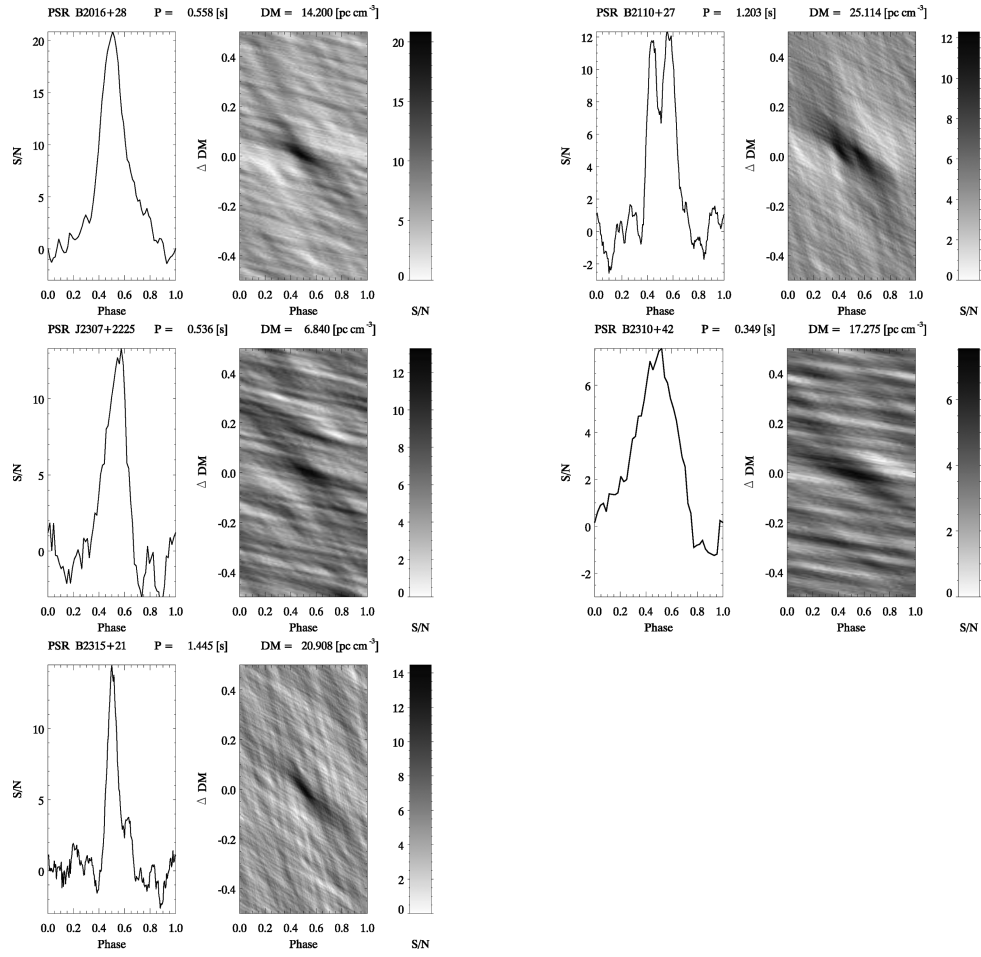


Figure A2 – continued

This paper has been typeset from a \LaTeX file prepared by the author.